ELECTRONIC COMPUTATION IN EAR OXIMETRY

by

G. R. Tait, B. Eng.

A thesis submitted to the Faculty of Graduate Studies and Research in partial fulfilment of the requirements for the degree of Master of Engineering.

Department of Electrical Engineering,
McGill University,
Montreal, Quebec.

April 1964

ABSTRACT

Ear oximetry is a technique used to determine the oxygen saturation of arterial blood in the intact man by a measurement of the absorption of red and infrared light passing through the ear. The withdrawal of an arterial sample of blood is not required.

A theoretical investigation has revealed some of the sources of error inherent in present earpiece optical arrangements which have limited the overall accuracy of the technique. These errors cannot be corrected for in practice but may be eliminated or minimized by improved earpiece construction. Several methods of evaluating the accuracy and reliability of both instantaneous and continuous absolute oxygen saturation measurements are suggested.

An analog computer for use with an existing ear oximeter to permit the continuous recording of oxygen saturation is also described.

ACKNOWLEDGEMENTS

The author wishes to express his appreciation and thanks to Dr. P. Sekelj and Dr. G. L. d'Ombrain for their supervision and guidance. Thanks are also due to Miss N. Anderson and Mr. M. Nathanson for their valuable discussions, and to Mr. B. Kwan for his assistance in proof-reading the thesis. The excellent typing was done by Miss D. Christmas.

This work was financed by the National Research Council of Canada.

TABLE OF CONTENTS

NOMENCLATURE

Chapters 1, 2, and 3

Subscripts (except where indicated below)

- λ wavelength
- i infrared wavelength(s)
- r red wavelength(s)
- X oxygen saturation
- o fully reduced (X = 0) hemoglobin or whole blood
- 1 fully oxygenated (X = 1.0) hemoglobin or whole blood

Main Symbols

- λ wavelength, in millimicrons ($m\mu$)
- I light intensity (watts/m^2)
- I_o incident light intensity (watts/m^2)
- A area (cm^2)
- ϵ absorption coefficient of hemoglobin or whole blood (litres/milli-mole/cm)
- C concentration (milli-moles/litre)
- d mean depth (cm)
- X relative oxygen saturation (by volume)
- x, y, z } cartesian co-ordinates (cm)
- E photocell voltage output with low resistance load (volts)
- E_o photocell voltage due to incident light (volts)

Main Symbols (cont.)

$G(\lambda)$ relative spectral response of filter

$H(\lambda)$ relative spectral response of photocell

$J(\lambda,y,z)$ light intensity distribution (watts/m^2/unit wavelength)

$J_o(\lambda,y,z)$ incident light intensity distribution (watts/m^2/mμ)

$\Delta x(y,z)$ deviation of total depth from the mean depth d (cm)

$\Delta\epsilon(\lambda)$ deviation of absorption coefficient at wavelength λ from that at a particular wavelength (litres/milli-mole/cm)

CHAPTER I

INTRODUCTION

A knowledge of the per cent oxygen saturation of arterial blood in vivo is necessary in studies involving the circulatory system in man, as well as in other areas of medicine. Several methods are now available which enable this determination to be made to a reasonable degree of accuracy. The principles involved are not new, the earliest use of colorimetric techniques being made by Drabkin [2] ✱ in 1932.

The most precise measurements of oxygen saturation are obtained by gasometric methods. The oxygen is chemically removed from the hemoglobin and is collected in gaseous form. The volume of gas is accurately measured and compared with that volume which the sample of blood would hold if it were 100 per cent saturated. This method is generally accepted as the standard today and is credited to Van Slyke and Neill [1] in 1924.

Several disadvantages are inherent in the Van Slyke technique although the results can be exceedingly good. One is the necessity to withdraw an arterial sample of blood which involves either an arterial puncture or catheterization of the heart. This procedure is time consuming and may be rather discomforting to the subject. The Van Slyke analysis itself, once the blood sample has been obtained,

✱ Reference to bibliography

requires about 20 minutes to one half hour to complete.

In an attempt to develop new methods which are more suited for clinical use as well as research, many investigators have turned to the use of the principles of colorimetry. Blood, when fully oxygenated, is bright red in color and when fully reduced (zero oxygen saturation) is very dark. A measure of the "color" of the blood is thus related to the relative oxygen saturation. Millikan [6] in 1942 developed an instrument using this principle to record continuously the oxygen saturation of blood in man. Others in succeeding years have expanded the method and improved its accuracy.

1.1 Spectrophotometric Methods

Spectrophotometric studies of blood can be made by considering a thin film (about 0.1 m.m.) suspended between two glass plates as illustrated in Fig. 1.1. Light of known wavelength and intensity is passed through the arrangement and a photoelectric cell is used to record the transmitted intensity. This arrangement is called a cuvette. With a knowledge of the light-absorbing properties of the blood in the cuvette it is possible to calculate the oxygen saturation of the sample from the light intensity measurements. A large number of experiments have been carried out by several investigators, mainly Drabkin, and have resulted in a sound basis for using colorimetric methods to determine oxygen saturation. One of the difficulties encountered is that measurements on whole blood have been dependent upon the specific instruments involved. Because whole blood is not a homogeneous light-absorbing

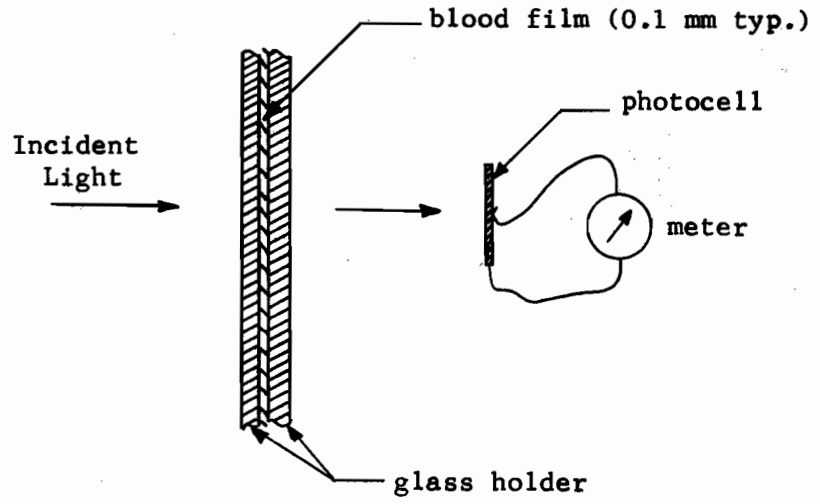

Fig. 1.1 A Cuvette Arrangement. Light of known wavelength and intensity is passed through a thin film of blood suspended between two glass plates. The photocell is used to measure the light intensity.

substance, but cellular in nature, the light passing through the blood is scattered by the red blood cells (erythrocytes) to some degree dependent upon instrument geometry and the initial scatter of the light source. Each instrument, therefore, must be individually calibrated against Van Slyke measurements.

One of the disadvantages present in the above method is also inherent in the Van Slyke analysis -- namely the procurement of an arterial blood sample. The measurement time, however, is greatly decreased. Also determinations must be made at discrete time intervals unless the cuvette is attached to the circulatory system in such a manner that the flow of blood is continuous.

1.2 The Ear as a Cuvette

To eliminate these inconveniences, the pinna or thin upper section of the human ear may be used as a crude cuvette. The blood is mainly arterial in this tissue when it is flushed, as very little oxygen exchange takes place. The advantages of such a system include no blood withdrawal, rapid and continuous measurements along with no discomfort to the subject. Various exercising tests, etc., may then be carried out which are not possible with cuvette or Van Slyke analysis. The advantages offered by ear oximetry indicate that due consideration be given to this technique.

The first instruments indicated only a relative measurement of oxygen saturation and were described by Millikan [6] and Goldie [7] in 1942. Other investigators produced instruments of similar design until 1949 when Wood [16] used a slightly different approach in excluding the blood from the ear by pressure to obtain an initial light intensity reading. This enabled an absolute measurement of oxygen saturation to be made. The accuracy and consistency in measurements are greater with the Wood type of oximeter. Sekelj [25], in 1951, considered that the ratio of the light intensities transmitted through the ear tissue (excluding the blood) in the two light bands employed (red and infrared) was a constant, invariant from ear to ear [44]. Absolute oxygen saturation measurements were then obtained without the necessity of excluding the blood from the ear, although a venous blood sample was required. Since the early 1950's new developments have been mainly concerned with improving the quality of the measuring equipment.

1.3 Reflection Oximeters

Reflection oximeters were first described by Brinkman and Zylstra [4] in 1938 as a method based on measurements of reflected light. The withdrawal of blood is still required, although the quantity is less than that for either Van Slyke or cuvette measurements. Rodrigo [29] in 1953 developed a theoretical treatment of the reflected light system and estimated that the errors involved were in the order of eight per cent. In recent years (1960-1962) reflection oximeters using glass fibre bundles to carry the light have been described [41, 47]. Measurements may be made in vivo, since the bundle of glass fibres is very small in diameter and may be inserted into the circulatory system through a Cournand arterial needle or a catheter. Thus, more detailed circulatory studies may be obtained where an ear measurement would not suffice.

1.4 Limitations in the Accuracy of Oximetry

Since the early papers on the spectrophotometric measurement of oxygen saturation, many instruments of similar design have been built and evaluated by independent groups. Certain characteristic results appear to have been obtained in each case. In cuvette oximetry there are errors which primarily arise from a combination of the instrument itself, and the failure of whole blood to behave like an ideal light absorbing medium. For a specific instrument, these errors may be minimized by proper calibration. In ear oximetry additional errors are introduced due to a combination of the instrument and the nonuniformity

of the ear tissue including the distribution of arteries and veins, etc. Since each ear is different, the latter errors cannot be eliminated by calibration. They may, however, be minimized by the proper design of equipment.

The results obtained from ear oximetry are less accurate than those from cuvette studies, a Van Slyke analysis being used as the standard in each case. An error of $\pm$ 5% in oxygen saturation from ear oximetry is not uncommon and in some cases the errors can be higher.

The main objective in the following chapters is a theoretical examination of some of the errors in oximetry and how to minimize them. The behavior of the measuring system itself in relation to accuracy is discussed along with some of the limitations in using the ear as a cuvette.

CHAPTER II

FUNDAMENTAL CONSIDERATIONS OF SPECTROPHOTOMETRIC MEASUREMENTS ON BLOOD AT DISCRETE WAVELENGTHS

The analysis of narrowband or monochromatic measurements on uniform films of blood is a special case of the general treatment developed in Chapter III. It is presented here as a summary of that theory found in the literature which is most often used as a basis for calculations in oximetry. This approach is extremely useful as it is applicable to practical cuvette measurements, and aids in the understanding of the technique as well as the errors and limitations of oximetry.

2.1 Transmission of Light Through an Ideal Absorbing Medium

The uniform cross-section of an ideal light-absorbing medium (Fig. 2.1) is subjected to a light source of wavelength λ and intensity $I_{o\lambda}$ (watts/m^2) at its surface. At a thin section, dx, the light intensities are I_λ and $I_\lambda + dI_\lambda$ as shown.

The quantity of light absorbed by the section dx is given by:

$$-dI_\lambda A = I_\lambda A dx \epsilon_\lambda \tag{2.1}$$

where ϵ_λ is the coefficient of absorption (m^{-1}) for that particular substance at wavelength λ. An exponential variation of light intensity with depth results from the solution of the differential equation (2.1), i.e.:

$$I_\lambda = I_{o\lambda} e^{-\epsilon_\lambda x} \tag{2.2}$$

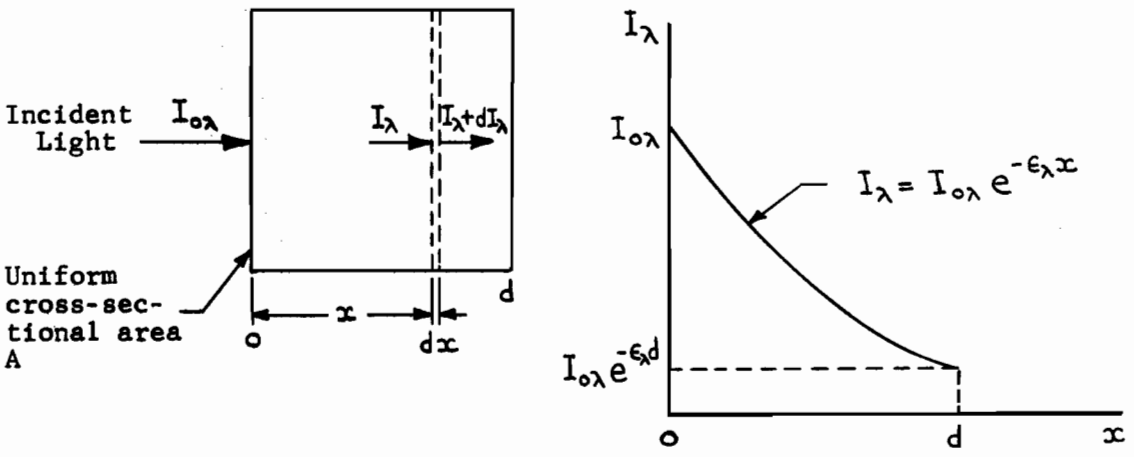

Fig. 2.1 Absorption of light by an ideal light absorbing medium.

This latter expression is known as the Bouguer-Lambert Law of Absorption (1729).

2.2 Transmission of Light Through Hemolyzed Blood

Hemoglobin is the substance in red blood cells (erythrocytes) which gives them their characteristic red color and their oxygen-carrying capability. The degree of red coloration of a cell will depend on the fraction of the total hemoglobin that is oxygenated. Cells which are darker in color contain less oxygen, i.e., oxygenated hemoglobin.

Whole blood consists mainly of plasma and erythrocytes which may be separated by centrifugation. When the red cells are suspended in distilled water they swell and burst due to osmosis and the hemoglobin solution inside is released. If necessary the cell debris may be removed by centrifugation. The resulting hemoglobin solution is called hemolyzed blood.

Hemoglobin itself is a complex organic molecule with a molecular weight of 66,800. It has been shown that a solution of hemoglobin behaves as an ideal light-absorbing medium following Beer's Law (Bouguer-Lambert Law applied to solutions). Expressed quantitatively

$$I_\lambda = I_{o\lambda} \exp\left[-\epsilon_{X\lambda} C d\right] \tag{2.3}$$

where: $I_{o\lambda}$ and I_λ are the incident and transmitted light intensities, respectively (watts/m^2)

d is the depth of the solution (cm.)

C is the concentration of the solution (milli-moles/litre)

$\epsilon_{X\lambda}$ is the absorption coefficient of pure hemoglobin and is a function of wavelength and oxygen saturation as indicated by the subscripts λ and X. (litres/milli-mole/cm)

Since a molecule of hemoglobin may be either oxygenated or reduced, it is possible and convenient to determine the absorption coefficients for these two states as a function of wavelength. This dependence is shown in Fig. 2.2. At 630 mμ (millimicrons) there is a large difference in the absorption coefficients for oxygenated and reduced hemoglobin, while at 805 mμ they are equal (isobestic point).

2.3 Transmission of Light Through Whole Blood

The transmission of light through whole blood has been shown through cuvette studies [15] to deviate somewhat from equation (2.3). These deviations are thought to arise primarily from the reflection and

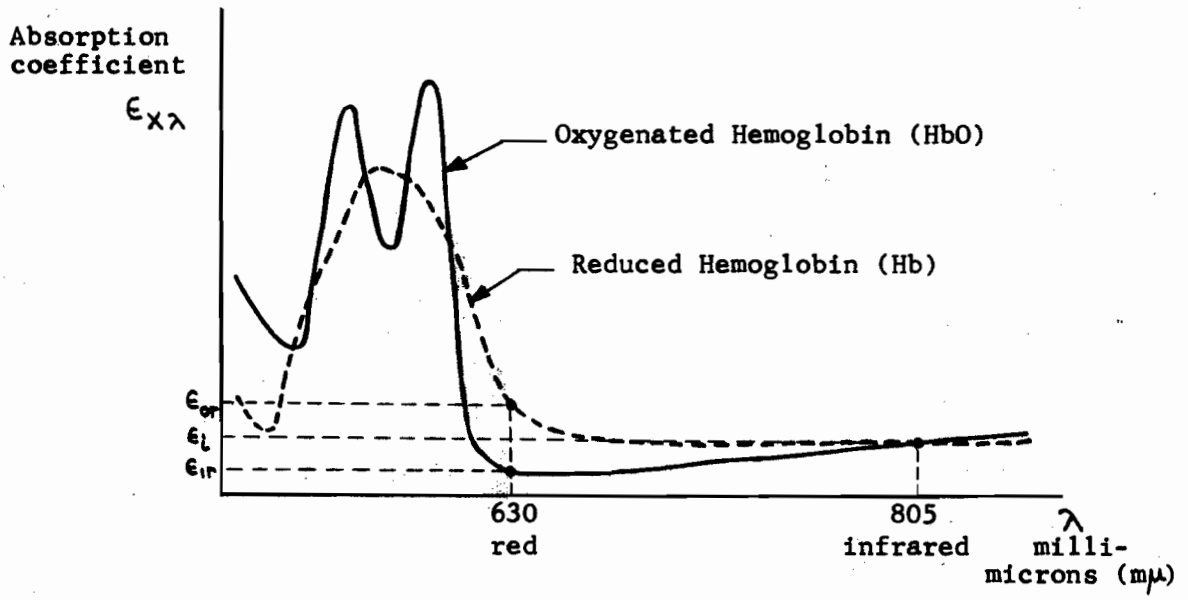

Fig. 2.2 Absorption coefficient of oxygenated and reduced hemoglobin solutions as a function of wavelength (millimicrons), the concentration of the solution being constant.

refraction of light passing through the cellular suspension. They are dependent upon the degree of scatter in the incident light as well as on the depth and particle concentration of the suspension. Thus the geometry of the cuvette and the rate of blood flow will have some effect on the behavior of the light transmission through whole blood, but for a fixed cuvette arrangement and constant flow these effects can easily be determined experimentally. The reproducibility of results among cuvettes of similar design will no doubt depend on the tolerances to which the instruments are matched.

At small cuvette depths and/or erythrocyte concentrations light is reflected and refracted through the blood and consequently

more light is passed through the suspension than is predicted from Beer's Law. At large depths and/or concentrations the suspension behaves more like an ideal absorbing medium and the application of equation (2.3) becomes more valid.

This suggests that Beer's Law be modified to some extent incorporating the deviations discussed above. If the cuvette depth is denoted by d (cm) and the hemoglobin concentration (proportional to the erythrocyte concentration) by C (milli-moles/litre), then we may write

$$I_\lambda = I_{o\lambda} \exp\left[- \epsilon_{\lambda X} C d f_\lambda(C,d,X) \right] \qquad (2.4)$$

as the modified form of equation (2.3).

The expression $f_\lambda(C,d,X)$ describes the behavior of the absorption coefficient for whole blood at wavelength λ as a function of concentration C, depth d, and oxygen saturation X. For hemolyzed blood $f_\lambda(C,d,X)$ is equal to 1.0. We have used this form of correction on the absorption coefficient $\epsilon_{\lambda X}$ as it allows us to express more easily the <u>deviation</u> of calculations on whole blood from those on hemolyzed blood.

It should be noted that the scatter of the incident light, as well as the geometry of the cuvette and the blood flow, are included in $f_\lambda(C,d,X)$. Consequently $f_\lambda(C,d,X)$ will not be unique but dependent on the equipment used, and the correspondence among instruments of the same design could only be evaluated by experiment.

2.4 Calculation of Relative Oxygen Saturation From Cuvette Measurements

1. Hemolyzed Blood

Light intensity measurements are made at two discrete wavelengths; 630 mμ and 805mμ in the red and infrared bands respectively. Let the absorption coefficient in the infrared band be ϵ_i (Fig. 2.2). It is the same for oxygenated and reduced hemoglobin. The absorption coefficients ϵ_{1r} and ϵ_{or} in the red band are for oxygenated and reduced hemoglobin, respectively, as denoted by the subscripts 1 and o. If a uniform cross-section of hemolyzed blood is considered, as illustrated in Fig. 2.3, the relative oxygen saturation by volume, X, is given by

$$X = \frac{d_1}{d_1 + d_o} = \frac{d_1}{d} \tag{2.5}$$

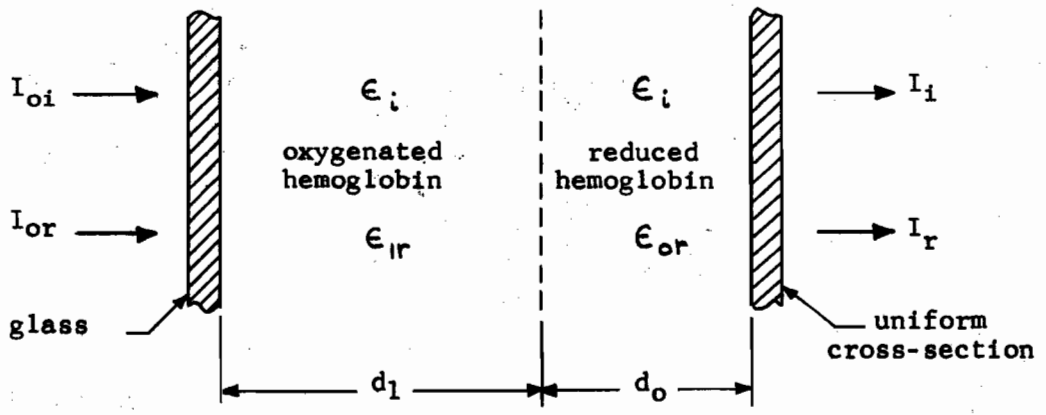

Fig. 2.3 Measurement of oxygen saturation in hemolyzed blood at two discrete wavelengths.

where: d_1 is the depth of oxygenated hemoglobin solution (cm)

d_o is the depth of reduced hemoglobin solution (cm)

$d = d_1 + d_o$ is the cuvette depth (cm)

In the infrared band equation (2.3) becomes

$$I_i = I_{oi} \exp\left[-\epsilon_i \, dC \right] \tag{2.6}$$

and in the red band since the exponents are additive

$$I_r = I_{or} \exp\left[-(\epsilon_{1r} d_1 + \epsilon_{or} d_o) C \right] \tag{2.7}$$

Taking logarithms of (2.6) and (2.7) we obtain

$$\ln \frac{I_i}{I_{oi}} = -\epsilon_i \, dC \tag{2.8}$$

and

$$\ln \frac{I_r}{I_{or}} = -\epsilon_{1r} d_1 C - \epsilon_{or}(d - d_1) C$$

$$= d\left[(\epsilon_{or} - \epsilon_{1r}) X - \epsilon_{or} \right] C \tag{2.9}$$

Eliminating the product dC from (2.8) and (2.9) yields

$$\frac{\ln I_r - \ln I_{or}}{\ln I_i - \ln I_{oi}} = -\frac{1}{\epsilon_i} \left[(\epsilon_{or} - \epsilon_{1r}) X - \epsilon_{or} \right] \tag{2.10}$$

thus

$$X = \frac{\epsilon_{or}}{\epsilon_{or} - \epsilon_{1r}} - \frac{\epsilon_i}{\epsilon_{or} - \epsilon_{1r}} \cdot \frac{\ln I_r - \ln I_{or}}{\ln I_i - \ln I_{oi}} \tag{2.11}$$

If readings of I_{or} and I_{oi} are made before the blood is inserted into the cuvette then X may be evaluated provided the absorption coefficients are known. Alternately, since the relation of X with $(\ln I_r - \ln I_{or})/(\ln I_i - \ln I_{oi})$ is a linear one, the constants may be determined empirically from a calibration curve using a gasometric measurement for X as the standard.

2. Whole Blood

Published data indicates that the application of equation (2.11) for calculating the oxygen saturation of whole blood gives less accurate results than those obtained from hemolyzed blood. This is due to the absorption coefficients not being constant but rather functions of cuvette depth, blood cell concentration, and oxygen saturation. Since the degree of interdependence of these three quantities is not yet fully known or understood, the superposition of exponents as in equation (2.7) cannot be assumed valid, although from experimental results the error should not be too great. Consequently for an accurate description of the oxygen saturation of whole blood, equation (2.4) must be used as a basis for any derivations.

For a specific cuvette arrangement of constant depth the transmission of light at the infrared wavelength is dependent on concentration only and is described by

$$I_i = I_{oi} \exp\left[-f_i(C)\right] \tag{2.12}$$

since the absorption coefficient is independent of oxygen saturation. Similarly the relation at a red wavelength becomes a function of concentration and oxygen saturation, viz:

$$I_r = I_{or} \exp\left[-f_r(C,X)\right] \tag{2.13}$$

We are required to know the concentration to evaluate both $f_i(C)$ and $f_r(C,X)$, and thus the use of two wavelengths to eliminate the dependence of oxygen saturation on d and C is redundant. X may be found from (2.13) only.

A choice of whether to use (2.13) or (2.11) with a correction factor can only be made once the functions $f_i(C)$ and $f_r(C,X)$ are known. In a practical system the overall accuracy as well as cost and ease of operation will be factors in deciding upon a one or two wavelength measurement.

CHAPTER III

THE EFFECT OF BROADBAND MEASUREMENTS ON NON-UNIFORM BLOOD FILMS - AN IDEALIZED APPROACH

The pinna, or thin upper section of the ear, may be considered as a crude cuvette. The blood is contained in the extensive vascular bed of small arteries, capillaries, and veins lying throughout the ear tissue. That part of the ear which does not contain blood will be called the "bloodless ear". For example, the ear would be considered bloodless if all the blood were replaced by a saline solution. This state can never be achieved in practice (in the human ear) but it is nevertheless a useful concept.

The blood contained in the flushed pinna is mainly arterial since there is little oxygen exchange with the ear tissue. If it were possible to make absolute light intensity measurements on the bloodless ear then the principles of a cuvette would apply directly and one might be able to consider equation (2.11) for calculation purposes. In practice such measurements are difficult to achieve without introducing some error, since the blood must be excluded by pressure. Distortion of the bloodless ear under pressure, as well as the fact that all the blood cannot be removed, will lead to errors in the measurement of oxygen saturation.

The problem of the bloodless ear is considered later. The analysis in this chapter will be concerned with the effect of non-monochromatic measurements on the non-uniform blood films which arise

from the uneven distribution of blood vessels and the inhomogeneity of the ear tissue.

3.1 Measuring Systems with Reference Co-ordinates

In Chapter II we dealt with measurements at discrete wavelengths. Many of the instruments presently employ broadband detecting devices as they have an advantage with respect to size, cost, and complexity of equipment over narrowband systems. The simplest and most useful detector is a solid-state photocell with the output short circuit current directly proportional to the incident light intensity. A light filter with an appropriate passband is used in front of the photocell to select the required wavelengths.

An illustration of a typical detector arrangement is shown in Fig. 3.1.

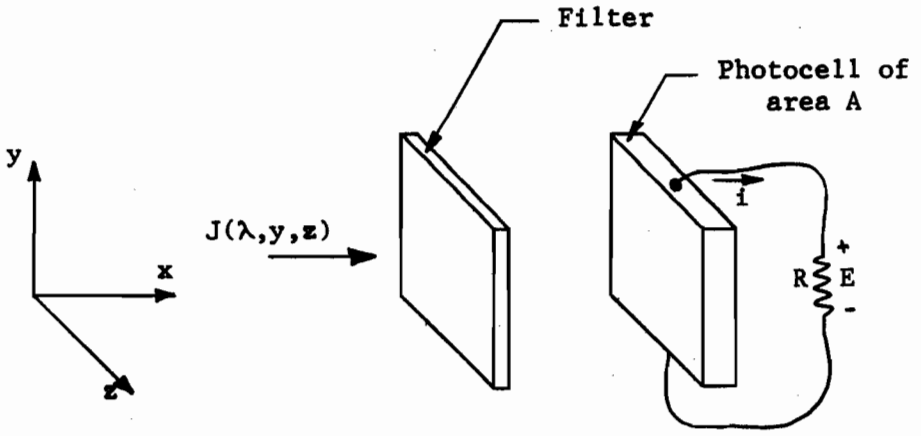

Fig. 3.1 Typical photocell detector arrangement with incident light intensity distribution $J(\lambda,y,z)$.

Light of intensity distribution $J(\lambda,y,z)$ (watts/m^2/unit wavelength) is incident on the filter-photocell combination. The load resistor R of the photocell is sufficiently small so that the output current of the cell is a linear function of the incident light intensity over the range considered. Thus the voltage E is also a linear function and may be evaluated from the expression (see Appendix 1)

$$E = k \int_A \int_\lambda G(\lambda)\, H(\lambda)\, J(\lambda,y,z)\, d\lambda\, dA \qquad (3.1)$$

where: $G(\lambda)$ is the relative response of the filter, assumed constant over its surface,

$H(\lambda)$ is the relative response of the photocell, assumed constant over its surface,

$J(\lambda,y,z)$ is the incident light intensity distribution, and

k is a constant for the particular filter-photocell combination.

The area integral is evaluated over the surface of the cell and the wavelength integral is evaluated over all wavelengths involved. It should be noted that the incident distribution $J(\lambda,y,z)$ is considered to be normal to the surfaces of the filter and photocell. If the light arrives at an angle then equation (3.1) may not directly apply. It is possible, however, to minimize this in practice by the use of a suitable light collimating arrangement.

3.2 Transmission of Light Through the Pinna

The depth of blood through an element of cross-section area, dA, of the pinna will change with position (y,z) over the surface. If we assume that measurements can be made on the bloodless ear alone, then we may consider the depth of blood as removed from the ear since superposition of optical densities applies. Fig. 3.2 illustrates the depth distribution of blood over an area A of the pinna.

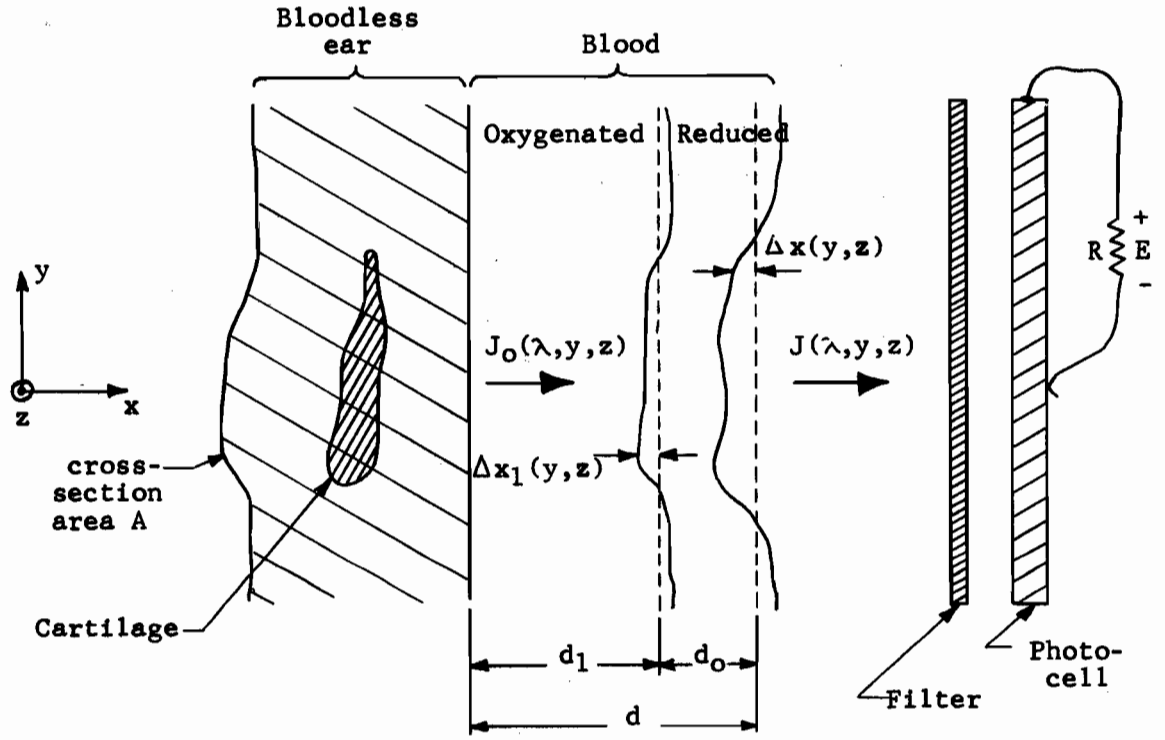

Fig. 3.2 Idealized Cross-Section of a Typical Pinna. The cross-section is in the y-z plane normal to the incident light. The depth of blood is less in the area containing the cartilage. $J_o(\lambda,y,z)$ is the light intensity distribution from the bloodless ear and $J(\lambda,y,z)$ is that for the complete cross-section (bloodless ear and blood).

The total depth is given by $\left[d + \Delta x(y,z)\right]$ where d is the mean value of the total depth over the area A. The depths of oxygenated and reduced blood are expressed in the same manner as $\left[d_1 + \Delta x_1(y,z)\right]$ and $\left[d_o + \Delta x_o(y,z)\right]$, respectively. It may be shown that

$$d = d_1 + d_o \tag{3.2}$$

and

$$\Delta x(y,z) = \Delta x_1(y,z) + \Delta x_o(y,z) \tag{3.3}$$

The voltage output of the photocell for the bloodless ear is expressed as

$$E_o = k \int_A \int_\lambda G(\lambda)\, H(\lambda)\, J_o(\lambda,y,z)\, d\lambda\, dA \tag{3.4}$$

and for the total cross-section including the blood as

$$E = k \int_A \int_\lambda G(\lambda)\, H(\lambda)\, J(\lambda,y,z)\, d\lambda\, dA \tag{3.1}$$

If we assume that Beer's Law applies to the transmission of light through an element of area containing blood, dA, then it is possible to express $J(\lambda,y,z)$ in terms of $J_o(\lambda,y,z)$, i.e.

$$J(\lambda,y,z) = J_o(\lambda,y,z) \exp\left[-\epsilon_X(\lambda)\, C \left\{d + \Delta x(y,z)\right\}\right] \tag{3.5}$$

where $\epsilon_X(\lambda)$ is the absorption coefficient of blood at saturation X and wavelength λ. We have not included the effects of light scattering since this behavior is probably not the same as that for cuvette studies

(equation (2.4)). In the actual ear the blood vessels are "intermixed" with the tissue and the scattering of light may be difficult to evaluate.

3.3 Evaluation of Relative Oxygen Saturation

The most general case, that of two photocells sampling two different cross-sections of the ear in the red and infrared bands, will be considered first. The subscripts i and r for infrared and red, respectively, will be used to denote which of the cross-sections and photocells are being considered. For the outputs of the bloodless ear we have from equation (3.4):

$$E_{oi} = k_i \int_A \int_\lambda G_i(\lambda)\, H_i(\lambda)\, J_{oi}(\lambda,y,z)\, d\lambda dA \tag{3.6}$$

and

$$E_{or} = k_r \int_A \int_\lambda G_r(\lambda)\, H_r(\lambda)\, J_{or}(\lambda,y,z)\, d\lambda dA \tag{3.7}$$

A combination of equations (3.1) and (3.5) will yield the outputs when the blood is included, viz

$$E_i = k_i \int_A \int_\lambda G_i(\lambda) H_i(\lambda) J_{oi}(\lambda,y,z) \exp\left[-C\left\{\epsilon_1(\lambda)\left[d_{1i} + \Delta x_{1i}(y,z)\right] + \epsilon_o(\lambda)\left[d_{oi} + \Delta x_{oi}(y,z)\right]\right\}\right] d\lambda dA \tag{3.8}$$

and

$$E_r = k_r \int_A \int_\lambda G_r(\lambda) H_r(\lambda) J_{or}(\lambda,y,z) \exp\left[-C\left\{\epsilon_1(\lambda)\left[d_{1r} + \Delta x_{1r}(y,z)\right] + \epsilon_o(\lambda)\left[d_{or} + \Delta x_{or}(y,z)\right]\right\}\right] d\lambda\, dA \qquad (3.9)$$

These expressions are a more general statement of Beer's Law and they reduce immediately to the simplified forms in Chapter II when monochromatic wavelengths and uniform depths are considered. It is obvious that in practice these equations cannot be evaluated, but it is possible to express the deviation of X as calculated from the general equations (3.8) and (3.9) from that value which would be determined if monochromatic wavelengths and uniform blood films were used. Although these deviations themselves cannot be evaluated, we are able to see what form they take, and thus how to eliminate or minimize them.

Consider first the absorption coefficients $\epsilon_1(\lambda)$ and $\epsilon_o(\lambda)$ for oxygenated and reduced blood respectively. These are shown as functions of wavelength in Fig. 3.3 and may be expressed as

$$\epsilon_1(\lambda) = \epsilon_{1r} + \Delta\epsilon_{1r}(\lambda) = \epsilon_i + \Delta\epsilon_{1i}(\lambda) \qquad (3.10)$$

and

$$\epsilon_o(\lambda) = \epsilon_{or} + \Delta\epsilon_{or}(\lambda) = \epsilon_i + \Delta\epsilon_{oi}(\lambda) \qquad (3.11)$$

It should be noted that ϵ_{1r} and ϵ_{or} are the absorption coefficients at some monochromatic wavelength in the red band. The same holds true for ϵ_i. We may now evaluate equation (3.8) which becomes:

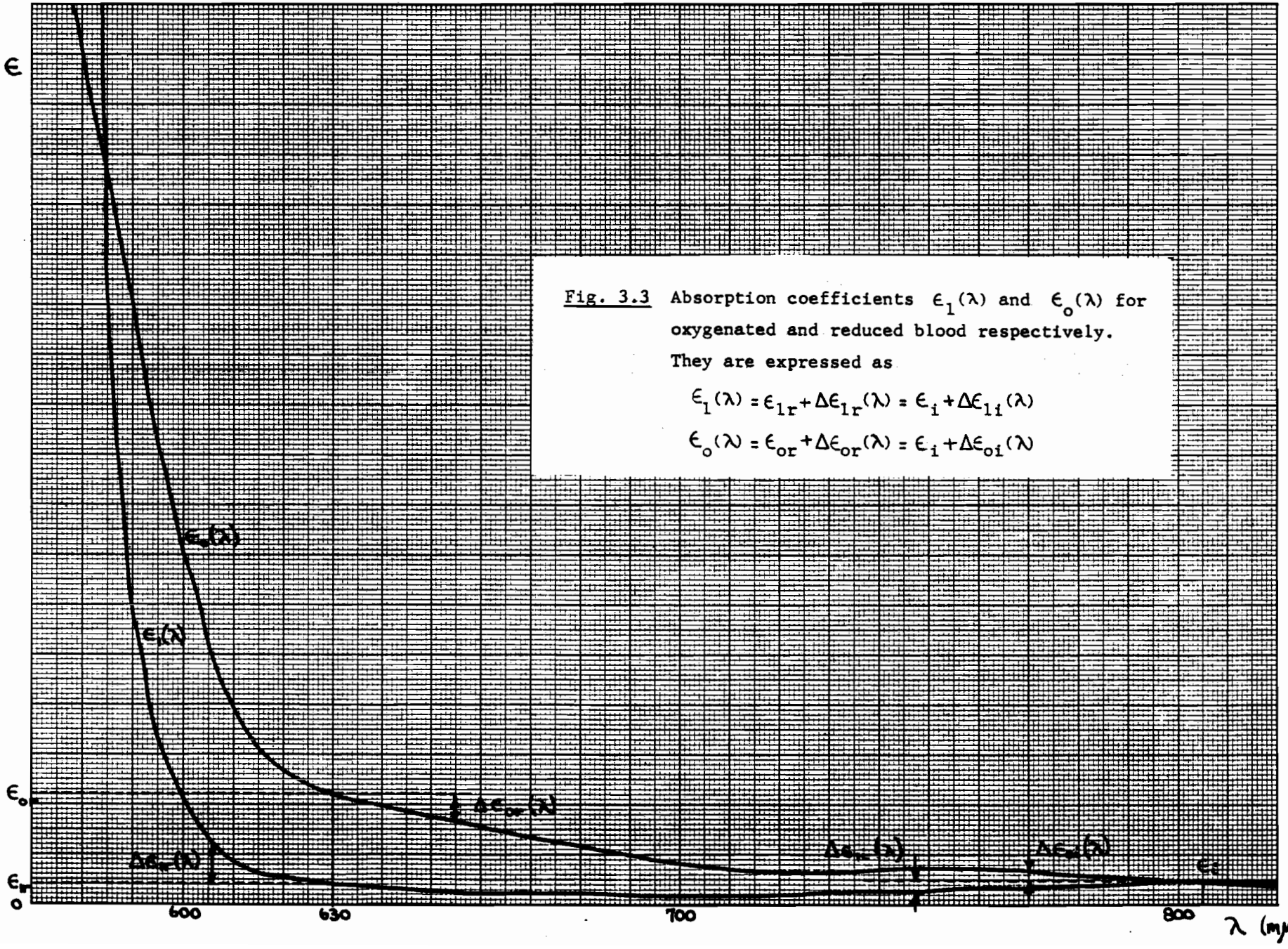

Fig. 3.3 Absorption coefficients $\epsilon_l(\lambda)$ and $\epsilon_o(\lambda)$ for oxygenated and reduced blood respectively. They are expressed as

$$\epsilon_l(\lambda) = \epsilon_{lr} + \Delta\epsilon_{lr}(\lambda) = \epsilon_i + \Delta\epsilon_{li}(\lambda)$$

$$\epsilon_o(\lambda) = \epsilon_{or} + \Delta\epsilon_{or}(\lambda) = \epsilon_i + \Delta\epsilon_{oi}(\lambda)$$

$$E_i = k_i \int_A \int_\lambda G_i(\lambda)\, H_i(\lambda)\, J_{oi}(\lambda, y, z)\ \exp\Big[-C\big\{[\epsilon_i + \Delta\epsilon_{ii}(\lambda)][d_{ii} + \Delta x_{ii}(y,z)] + [\epsilon_i + \Delta\epsilon_{oi}(\lambda)][d_{oi} + \Delta x_{oi}(y,z)]\big\}\Big]\, d\lambda\, dA \quad (3.12)$$

$$= \exp\Big[-C\epsilon_i (d_{ii} + d_{oi})\Big]\, k_i \int_A \int_\lambda G_i(\lambda)\, H_i(\lambda)\, J_{oi}(\lambda, y, z)\ \exp\Big[-C \big\{ d_{ii}\, \Delta\epsilon_{ii}(\lambda) + d_{oi}\, \Delta\epsilon_{oi}(\lambda) + \epsilon_i [\Delta x_{ii}(y,z) + \Delta x_{oi}(y,z)] + \Delta\epsilon_{ii}(\lambda)\, \Delta x_{ii}(y,z) + \Delta\epsilon_{oi}(\lambda)\, \Delta x_{oi}(y,z)\big\}\Big]\, d\lambda\, dA \quad (3.13)$$

Therefore

$$E_i = E_{oi}\, R_i\ \exp\Big[-C\epsilon_i (d_{ii} + d_{oi})\Big] \quad (3.14)$$

Where

$$R_i = \frac{\displaystyle\int_A \int_\lambda G_i(\lambda)\, H_i(\lambda)\, J_{oi}(\lambda, y, z)\ \exp\Big[-C\big\{d_{ii}\, \Delta\epsilon_{ii}(\lambda) + d_{oi}\, \Delta\epsilon_{oi}(\lambda)\big\}\Big]\ \exp\Big[-C\epsilon_i\big\{\Delta x_{ii}(y,z) + \Delta x_{oi}(y,z)\big\}\Big]\ \exp\Big[-C\big\{\Delta\epsilon_{ii}(\lambda)\, \Delta x_{ii}(y,z) + \Delta\epsilon_{oi}(\lambda)\, \Delta x_{oi}(y,z)\big\}\Big]\, d\lambda\, dA}{\displaystyle\int_A \int_\lambda G_i(\lambda)\, H_i(\lambda)\, J_{oi}(\lambda, y, z)\, d\lambda\, dA} \quad (3.15)$$

Similarly for the red cross-section:

$$E_r = k_r \int_A \int_\lambda G_r(\lambda)\, H_r(\lambda)\, J_{or}(\lambda,y,z)\, \exp\Big[-C\big\{[\epsilon_{ir}+\Delta\epsilon_{ir}(\lambda)][d_{ir}+\Delta x_{ir}(y,z)] + [\epsilon_{or}+\Delta\epsilon_{or}(\lambda)][d_{or}+\Delta x_{or}(y,z)]\big\}\Big]\, d\lambda\, dA$$

$$= \exp\left[-C(\epsilon_{ir} d_{ir} + \epsilon_{or} d_{or})\right] k_r \int_A \int_\lambda G_r(\lambda)\, H_r(\lambda)\, J_{or}(\lambda,y,z)\, \exp\Big[-C\big\{d_{ir}\,\Delta\epsilon_{ir}(\lambda) + d_{or}\,\Delta\epsilon_{or}(\lambda) + \epsilon_{ir}\,\Delta x_{ir}(y,z) + \epsilon_{or}\,\Delta x_{or}(y,z) + \Delta\epsilon_{ir}(\lambda)\,\Delta x_{ir}(y,z) + \Delta\epsilon_{or}(\lambda)\,\Delta x_{or}(y,z)\big\}\Big]\, d\lambda\, dA$$

Therefore

$$E_r = E_{or}\, R_r\, \exp\left[-C\,(\epsilon_{ir} d_{ir} + \epsilon_{or} d_{or})\right] \tag{3.16}$$

Where

$$R_r = \frac{\displaystyle\int_A \int_\lambda G_r(\lambda)\, H_r(\lambda)\, J_{or}(\lambda,y,z)\, \exp\Big[-C\big\{d_{ir}\,\Delta\epsilon_{ir}(\lambda) + d_{or}\,\Delta\epsilon_{or}(\lambda)\big\}\Big] \exp\Big[-C\big\{\epsilon_{ir}\,\Delta x_{ir}(y,z) + \epsilon_{or}\,\Delta x_{or}(y,z)\big\}\Big] \exp\Big[-C\big\{\Delta\epsilon_{ir}(\lambda)\,\Delta x_{ir}(y,z) + \Delta\epsilon_{or}(\lambda)\,\Delta x_{or}(y,z)\big\}\Big]\, d\lambda\, dA}{\displaystyle\int_A \int_\lambda G_r(\lambda)\, H_r(\lambda)\, J_{or}(\lambda,y,z)\, d\lambda\, dA} \tag{3.17}$$

Beer's Law is now immediately recognized in equations (3.14) and (3.16) with the addition of terms R_i and R_r respectively. These modifying terms will be called the <u>effective errors</u>. They arise from the use of a broadband spectrum and non-uniform blood depth distributions.

In order to calculate oxygen saturation we need only consider equations (3.14) and (3.16). Let the difference in the mean blood depths of the red and infrared cross-sections be Δd. Thus

$$\Delta d = d_i - d_r \tag{3.18}$$

$$= d_i - (d_{1r} + d_{or}) \tag{3.19}$$

and equation (3.14) becomes

$$E_i = E_{oi} R_i \exp\left[-C \epsilon_i d_r (1 + \frac{\Delta d}{d_r})\right] \tag{3.20}$$

From (3.16) we obtain

$$E_r = E_{or} R_r \exp\left[-C d_r \left\{(\epsilon_{1r} - \epsilon_{or}) X + \epsilon_{or}\right\}\right] \tag{3.21}$$

Eliminating d_r from (3.20) and (3.21) and solving for X yields

$$X = \frac{\epsilon_{or}}{\epsilon_{or} - \epsilon_{1r}} - \frac{\epsilon_i}{\epsilon_{or} - \epsilon_{1r}} (1 + \frac{\Delta d}{d_r}) \cdot \frac{\ln E_r - \ln E_{or} - \ln R_r}{\ln E_i - \ln E_{oi} - \ln R_i} \tag{3.22}$$

This relation for X should be compared with equation (2.11). Under conditions similar to those for which (2.11) was derived the effective

errors in (3.22) reduce to zero.

Since we are interested in evaluating the deviations due to the error terms from the ideal behavior of X at discrete wavelengths and uniform blood depths, we may write (3.22) in a more convenient form. Let us define

$$R = \frac{\ln E_r - \ln E_{or}}{\ln E_i - \ln E_{oi}} \tag{3.23}$$

An algebraic manipulation of (3.22) yields

$$X = \frac{\epsilon_{or}}{\epsilon_{or} - \epsilon_{1r}} - \frac{\epsilon_i}{\epsilon_{or} - \epsilon_{1r}} \cdot \left(1 + \frac{\Delta d}{d_r}\right) R - F(X) \tag{3.24}$$

where

$$F(X) = \frac{\frac{\epsilon_i}{\epsilon_{or} - \epsilon_{1r}} \left(1 + \frac{\Delta d}{d_r}\right) \ln R_r + \left(X - \frac{\epsilon_{or}}{\epsilon_{or} - \epsilon_{1r}}\right) \ln R_i}{C \epsilon_i d_r \left(1 + \frac{\Delta d}{d_r}\right) - \ln R_i} \tag{3.25}$$

From (3.24) we see that if we do not use discrete wavelengths, uniform blood depth distributions, or equal mean blood depths in the red and infrared sections, then X is described by the addition of two terms: $\left(1 + \frac{\Delta d}{d_r}\right)$ and $F(X)$. These terms are impossible to evaluate in practical measurements on the ear. In cuvette measurements it should be theoretically possible to correct for these errors although highly impractical. The term $F(X)$ is a function of oxygen saturation, not

only as indicated in (3.25) but also through R_r and R_i as will be shown in the next sections.

3.4 The Effects of Practical Measurements on Oxygen Saturation

Oxygen saturation, X, must be determined from readings made on the ear. These are E_r, E_i, E_{oi}, and E_{or}, which are incorporated into the parameter R in (3.23). The unwanted terms, $(1 + \frac{\Delta d}{d_r})$ and F(X), constitute sources of error from the commonly used expression (2.11). They are unwanted because they are impossible to correct for in practice. We can show, however, the effect of each of the sources of error separately and also indicate methods of minimizing or eliminating them.

1. Error from sampling two different cross-sections

One result of sampling through two different sections of the pinna in the red and infrared bands is immediately evident from (3.24). The relative error $\Delta d/d_r$ may be either positive or negative and will vary with position on the pinna as well as from ear to ear. It cannot be accounted for in practice but may easily be eliminated by sampling through the same cross-sectional area in the red and infrared bands. The qualitative effect is one of generating less confidence in lower values of oxygen saturation, giving rise to a larger spread in this area. This is illustrated in Fig. 3.4. This term also appears in F(X) but its actual effect is difficult to interpret since F(X) depends on many other factors.

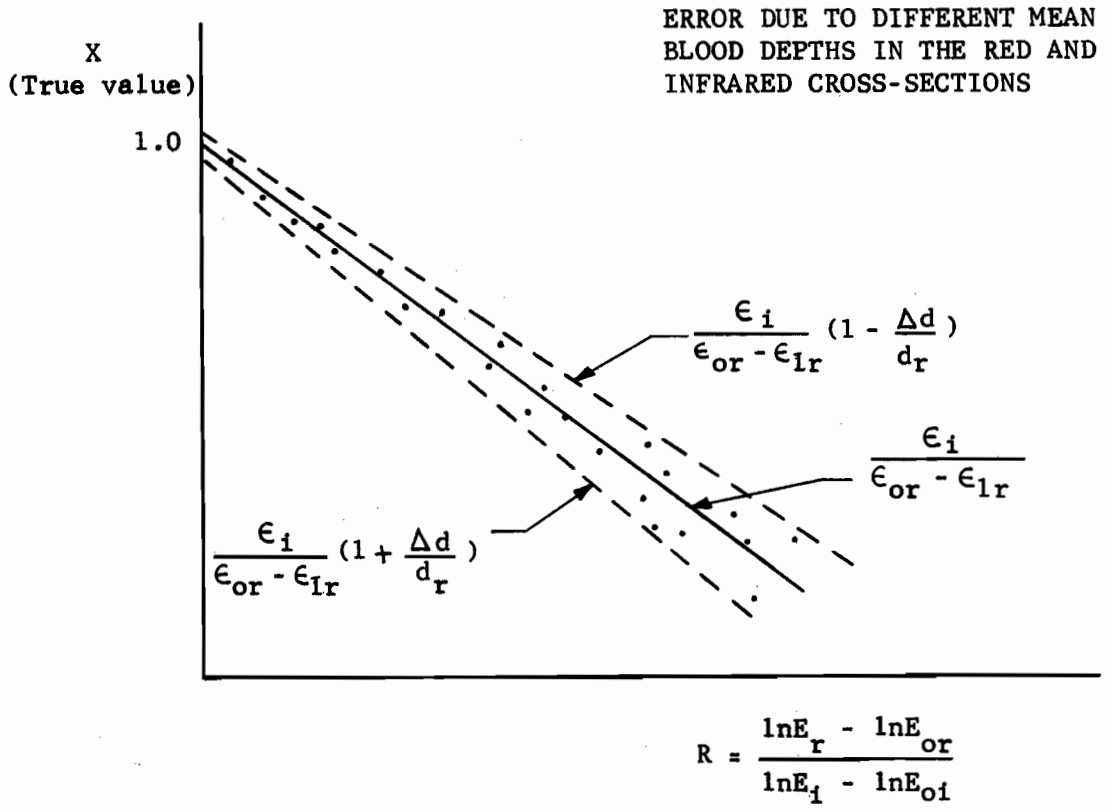

Fig. 3.4 The variation of the true value of oxygen saturation X against the measured ratio R. The difference in the mean blood depth in the red and infrared cross-sections gives rise to a lack of confidence in R. The change in slope of (3.26) is shown by the dotted lines. If the same cross-section is used for each band, then all calibration points should lie along the solid line (neglecting other sources of error).

2. Error from non-uniform blood depth distributions

The effects of R_i and R_r on oxygen saturation measurements are difficult to interpret by inspection since the expressions are rather involved. By considering practical measurements made

through the same cross-sectional area A at appropriate nearly monochromatic wavelengths in the red and infrared bands we may simplify the error term F(X) to include only the effects of non-uniform light intensities and blood depth distributions. For the infrared cross-section under these assumptions equation (3.15) reduces to

$$R_i = \frac{\int_A J_{oi}(y,z)\exp\left[-C\epsilon_i \Delta x(y,z)\right] dA}{\int_A J_{oi}(y,z)\, dA} \tag{3.26}$$

since by definition

$$\Delta x(y,z) = \Delta x_1(y,z) + \Delta x_o(y,z) \tag{3.27}$$

$$= \Delta x_{1i}(y,z) + \Delta x_{oi}(y,z) \tag{3.28}$$

$J_{oi}(y,z)$ is the incident light intensity distribution on the blood over the sampled area A at the nearly monochromatic infrared wavelength (805 mμ). Similarly the red term (3.17) becomes

$$R_r = \frac{\int_A J_{or}(y,z)\exp\left[-C\{\epsilon_{1r}\Delta x_1(y,z) + \epsilon_{or}\Delta x_o(y,z)\}\right]dA}{\int_A J_{or}(y,z)\, dA} \tag{3.29}$$

If both the effective errors R_i and R_r are equal to 1.0, then F(X) in the expression for X, (3.24), is zero and oxygen saturation may be accurately determined from the measured ratio R. Thus R_i and R_r as given by equations (3.26) and (3.29) should represent

the main sources of error under the above assumptions, provided, of course, that the initial readings on the blood film, E_{or} and E_{oi}, are accurately obtainable. In fact E_{or} and E_{oi} will depend on the bloodless ear tissue itself and can only be obtained in a true sense by replacing the blood in the ear by a non-absorbing medium. Because the ear tissue (without blood) is nonhomogeneous it is difficult to assess the effect of the size of the sampled area on $F(X)$. However, by examining the very special case outlined below we may see qualitatively the behavior of the effective errors R_i and R_r and their relation to the size of the sampled area A.

Let us consider the behavior of an ideal ear. We shall assume that the bloodless ear is itself homogeneous and has throughout the sampled volume a constant coefficient of absorption, α, in the infrared band. Only the analysis for infrared wavelengths is attempted here as that for red wavelengths is similar. Further, let the total depth of the ear, d_e, be a constant independent of position (y,z). This is illustrated in Fig. 3.5 A. Several regions with blood densities above and below the average value are shown (shaded areas). When the bloodless ear and the blood are considered separately (Fig. 3.5 B), the total depth d_e through any element of cross-section must equal the sum of the depths of the bloodless ear tissue and the blood. To simplify the calculations we shall let the incident light intensity distribution on the ear, J'_{oi}, be a constant independent of wavelength and position. The depth of the bloodless ear is thus $d_e - \left[d + \Delta x(y,z)\right]$ and from the law of light

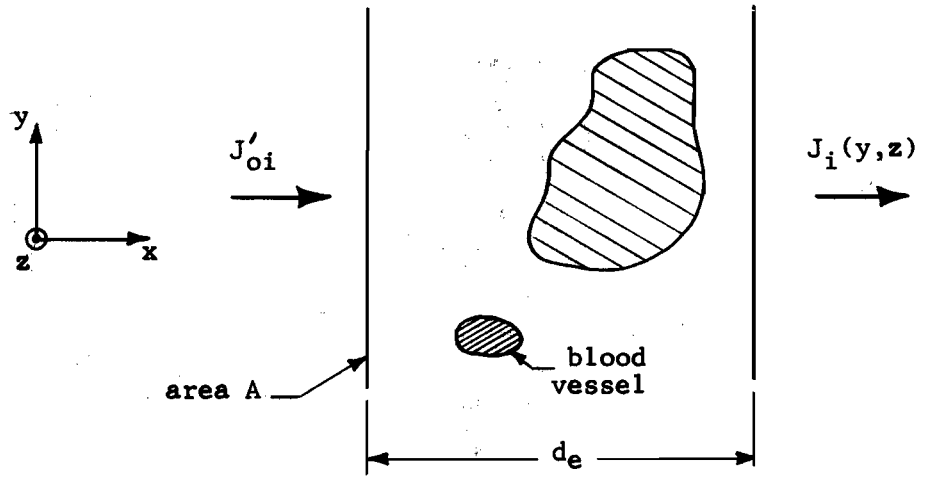

Fig. 3.5 A Cross-section of an ideal ear of uniform depth d_e in which the large shaded area represents a region containing less blood. The incident and transmitted light intensity distributions are J'_{oi} and $J_i(y,z)$ respectively in the infrared band.

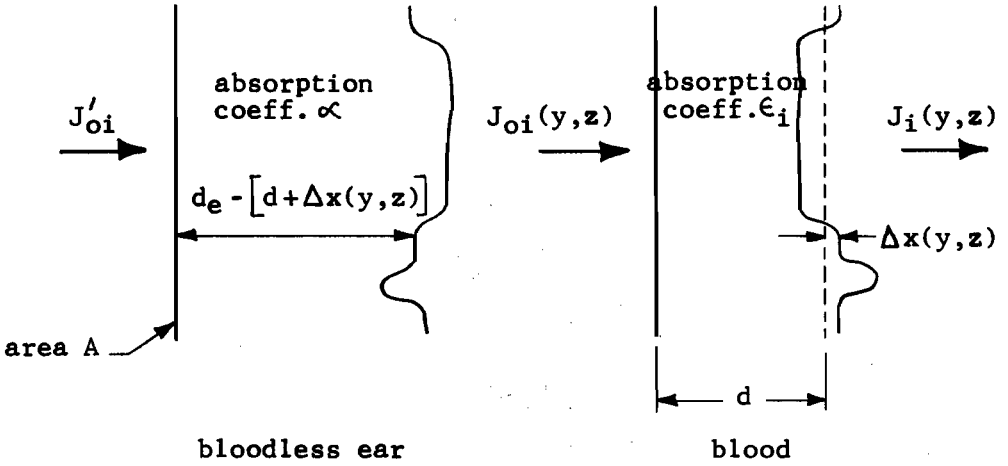

Fig. 3.5 B Cross-section of Fig. 3.5 A separated into sections of bloodless ear and blood. The mean blood depth of the non-uniform blood depth distribution is denoted by d.

transmission applied to the bloodless ear we have

$$J_{oi}(y,z) = J'_{oi} \exp\left[-\alpha\left\{d_e - d - \Delta x(y,z)\right\}\right] \tag{3.30}$$

$$= J'_{oi} \exp\left[-\alpha(d_e - d)\right]\exp\left[\alpha\Delta x(y,z)\right] \tag{3.31}$$

Substituting (3.31) in the expression for R_i (3.26) yields

$$R_i = \frac{\frac{1}{A}\int_A \exp\left[(\alpha - C\epsilon_i)\,\Delta x(y,z)\right] dA}{\frac{1}{A}\int_A \exp\left[\alpha\Delta x(y,z)\right] dA} \tag{3.32}$$

and by considering the first three terms in the expansions for the exponentials in (3.32), the term R_i reduces to

$$R_i \cong \frac{1 + \frac{(\alpha - C\epsilon_i)^2}{2!}\,\frac{1}{A}\int_A \Delta x^2(y,z)\, dA}{1 + \frac{\alpha^2}{2!}\,\frac{1}{A}\int_A \Delta x^2(y,z)\, dA} \tag{3.33}$$

since by definition of the mean blood depth d,

$$\int_A \Delta x(y,z)\, dA = 0 \tag{3.34}$$

The integrals in equation (3.33) describe the variance of the blood depth distribution over the sampled area A. This variance will always exist and will be different for each ear sampled. Therefore R_i will always be different from 1.0 and consequently will contribute an error, even for ideal ears. We observe that the larger

the sampling area A, the smaller the spread in the variances over a large number of sampled ears, provided that the frequency distribution of $\Delta x(y,z)$ over the area A is roughly the same for each ear. In the case of ideal ears, then, a smaller spread in the effective error R_i would be expected over many subjects if the sampling area were made large. It should be noted that sampling a very small area would, as this area approached zero, make R_i equal to 1.0 and thus eliminate completely the error discussed above. In fact if the area sampled is sufficiently smaller than the smallest deviation of $\Delta x(y,z)$ then R_i should always be close to 1.0.

For real ears, α will vary throughout the ear although this variation will be minimized if the sampled area is small. It also appears that since bloodless ears are nonhomogeneous the dominant error when large areas are sampled may be due to the bloodless ear rather than the blood depth distribution. In a practical system these effects can only be investigated by experiments using different sampling areas. At this point no definite conclusion can be drawn, except that the optimum sampling area, if there is any, may depend on the actual instrument involved since the initial light intensity distribution on the ear will probably not be a constant, nor will be the response of the photocell over its surface. Fig. 3.6 shows the effect these errors have on the determination of oxygen saturation. For a true oxygen saturation X there will be a lack of confidence in the abscissa of the

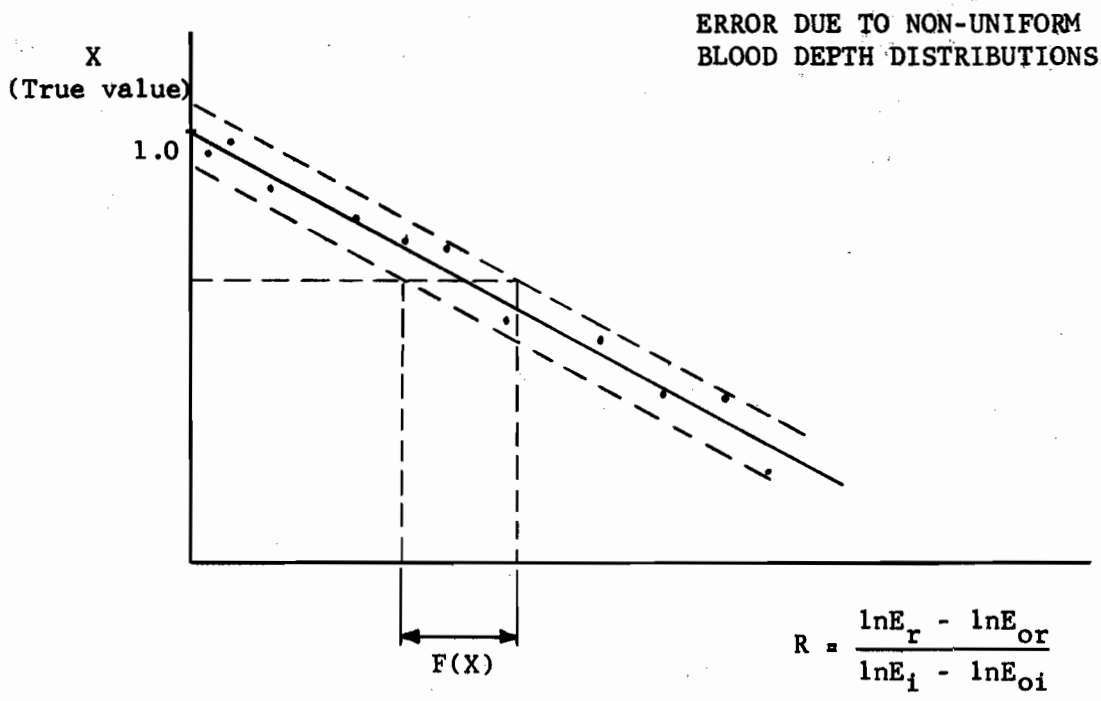

Fig. 3.6 The true oxygen saturation X plotted against the ratio R. E_r, E_{or}, E_i, and E_{oi} are "measured" values. The possible error in R due to non-uniform blood depth distributions is denoted by F(X). A resulting calibration curve as shown above would have some uncertainty due to this effect as shown by the dotted lines.

instrument calibration curve, and a quantitative estimation of these deviations can only be arrived at by experimental measurements.

3. Effects of non-monochromatic measurements

An analysis of the effect of broadband measurements is possible if the depth distribution is constant. This is the case in cuvette measurements for which $\Delta x_{oi}(y,z)$, $\Delta x_{1i}(y,z)$, $\Delta x_{or}(y,z)$,

$\Delta x_{1r}(y,z)$ are each zero. Further, let us consider that the same cross-section is being sampled at each wavelength so that $d_i = d_r = d$. Then equation (3.15) reduces to

$$R_i = \frac{\int_A \int_\lambda G_i(\lambda)\, H_i(\lambda)\, J_{oi}(\lambda,y,z) \exp\left[-C\left\{d_{1i}\Delta\epsilon_{1i}(\lambda) + d_{oi}\,\Delta\epsilon_{oi}(\lambda)\right\}\right] d\lambda\, dA}{\int_A \int_\lambda G_i(\lambda)\, H_i(\lambda)\, J_{oi}(\lambda,y,z)\, d\lambda\, dA} \tag{3.35}$$

$$= \frac{\int_A \int_\lambda G_i(\lambda)\, H_i(\lambda)\, J_{oi}(\lambda,y,z) \exp\left[-Cd\left\{\left[\Delta\epsilon_{1i}(\lambda) - \Delta\epsilon_{oi}(\lambda)\right] X + \Delta\epsilon_{oi}(\lambda)\right\}\right] d\lambda dA}{\int_A \int_\lambda G_i(\lambda)\, H_i(\lambda)\, J_{oi}(\lambda,y,z)\, d\lambda dA} \tag{3.36}$$

To further simplify (3.36) let us assume that $J_{oi}(\lambda,y,z)$ has the same spectral distribution over the surface of the blood so that

$$J_{oi}(\lambda,y,z) = j(\lambda)\, J(y,z) \tag{3.37}$$

where $j(\lambda)$ is the relative spectral distribution. Since we are sampling the same area in each band then (3.37) applies equally well in the red. Thus for the infrared, equation (3.36) becomes

$$R_i = \frac{\int_\lambda G_i(\lambda)\, H_i(\lambda)\, j(\lambda) \exp\left[-Cd\left\{\left[\Delta\epsilon_{1i}(\lambda) - \Delta\epsilon_{oi}(\lambda)\right] X + \Delta\epsilon_{oi}(\lambda)\right\}\right] d\lambda}{\int_\lambda G_i(\lambda)\, H_i(\lambda)\, j(\lambda)\, d\lambda} \tag{3.38}$$

and in the red band we similarly obtain

$$R_r = \frac{\int_\lambda G_r(\lambda)\, H_r(\lambda)\, j(\lambda) \exp\left[-Cd\left\{\left[\Delta\epsilon_{1r}(\lambda) - \Delta\epsilon_{or}(\lambda)\right] X + \Delta\epsilon_{or}(\lambda)\right\}\right] d\lambda}{\int_\lambda G_r(\lambda)\, H_r(\lambda)\, j(\lambda)\, d\lambda} \tag{3.39}$$

Also from (3.25) and (3.24)

$$F(X) = \frac{\frac{\epsilon_i}{\epsilon_{or} - \epsilon_{1r}} \ln R_r + (X - \frac{\epsilon_{or}}{\epsilon_{or} - \epsilon_{1r}}) \ln R_i}{Cd\epsilon_i - \ln R_i} \tag{3.40}$$

and

$$X = \frac{\epsilon_{or}}{\epsilon_{or} - \epsilon_{1r}} - \frac{\epsilon_i}{\epsilon_{or} - \epsilon_{1r}} R - F(X) \tag{3.41}$$

If we now plot the true value of X against the measured ratio R we shall not obtain a linear relationship as (2.11) indicates, but instead we must subtract F(X) from the intercept with the ordinate. This is illustrated in Fig. 3.7. As narrower bandwidths are used F(X) becomes smaller and smaller until at discrete wavelengths the straight line relation results.

4. Behavior of Cumulative Errors

The cumulative effect of the errors in the last three sections is difficult to evaluate in a quantitative sense. However, we may expect that from the result of many oxygen saturation measurements the net behavior is some superposition of Figs. 3.4, 3.6 and 3.7. In practice this has generally been the case. The relation for X vs. R is curved -- the curvature being less pronounced at narrowband measurements. More confidence is obtained for values of oxygen saturation near 100 per cent than near 60 per cent. In general there is a lack of confidence over the whole range of X, and some of the possible reasons for this have been outlined above.

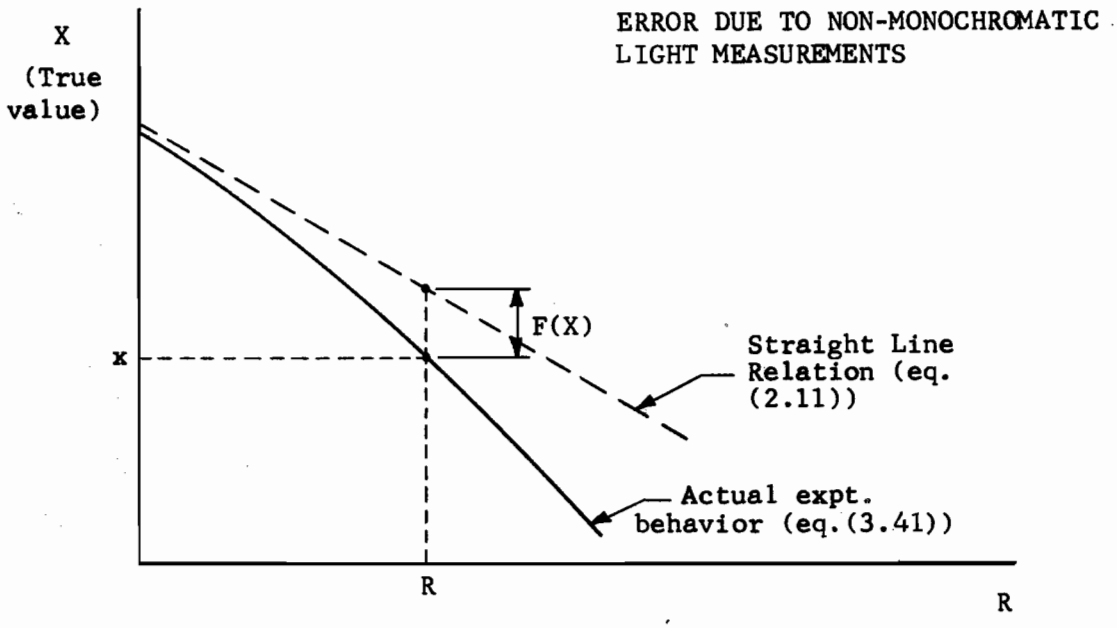

Fig. 3.7 The behavior of oxygen saturation X with the measured ratio R. The experimental curve is shown as the solid line. It is obtained by subtracting F(X) in equation (3.41) from the straight line relation of equation (2.11).

Fig. 3.8 illustrates the typical spread predicted above and obtained over the years in the literature.

3.5 Optimum Measuring System

The analysis presented in the past sections concerns only ideal systems. Accurate cuvette measurements may approach this in practice -- certainly measurements on the ear do not. However, we can do no better than measurements on an ideal system. The light scattering effects of blood and tissue, as well as the problem of the bloodless ear, will increase our lack of confidence

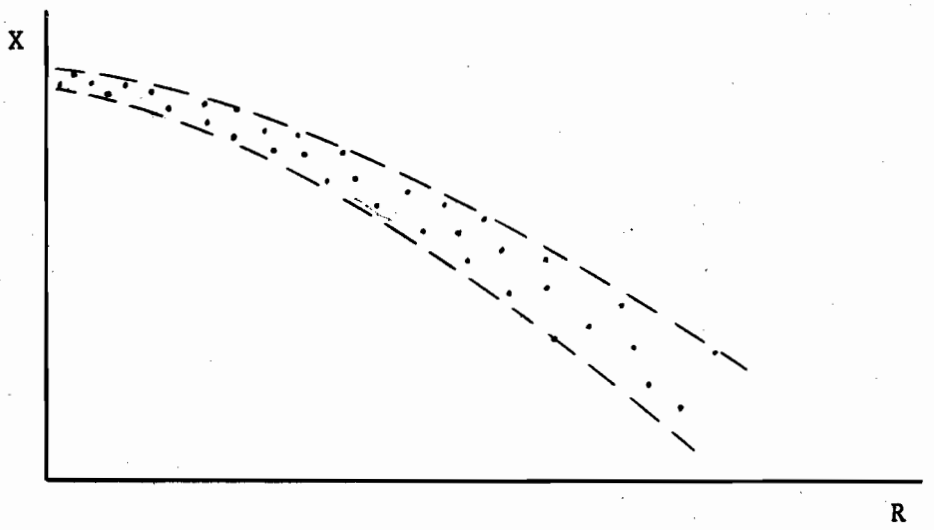

Fig. 3.8 Experimental behavior of X and R. This curve results from a superposition of Figs 3.4, 3.5 and 3.6. The dashed lines show roughly the extent of the lack of confidence in the relation. (Drawing not to scale.)

in this method.

Several things have become apparent, and are listed below:

1. The only practical spectrophotometric relation which is useful in evaluating oxygen saturation is R (eq. (3.23)).

2. Correction of the linear relation (2.11) for non-uniform blood depth distributions and broadband measurements is probably impossible.

3. The error terms can be significant. For example, at monochromatic wavelengths and uniform depth distributions, if $\Delta d = \pm \cdot 05\, d_r$ (this certainly is not unreasonable when sampling through two different cross-sections of many ears), we immediately

have a $\pm$ 5% lack of confidence in R from equation (3.24).

4. For continuous computation of X a straight line relation is desirable.

5. It is impossible to clearly evaluate other potential sources of error, such as light scattering and the problem of the bloodless ear, until the above errors are minimized or, preferably, eliminated.

CHAPTER IV

THE PROBLEM OF THE BLOODLESS EAR

The analysis carried out in Chapters II and III has been based on the following fact: oxygen saturation can be determined from two measurements made with the photocell in the red and infra-red bands, one before a film of blood has been introduced into the light path, and one after. The difficulty in using the ear as a cuvette is in obtaining true readings when the ear is "bloodless". These readings will always be in error since the bloodless ear is distorted under pressure and all the blood cannot be removed by compression. We shall assume in this section for purposes of analyzing the bloodless ear that an instrument is available which eliminates or minimizes the errors discussed in Chapter III. Therefore, under these conditions oxygen saturation may be expressed as

$$X = \frac{\epsilon_{or}}{\epsilon_{or} - \epsilon_{1r}} - \frac{\epsilon_{i}}{\epsilon_{or} - \epsilon_{1r}} \cdot \frac{\ln E_r - \ln E_{or}}{\ln E_i - \ln E_{oi}} \qquad (4.1)$$

providing E_r, E_i, E_{or} and E_{oi} are accurately measureable.

4.1 Instantaneous Measurement of Oxygen Saturation

By an instantaneous measurement of oxygen saturation we imply that the measurement is made sufficiently fast so that the arterial oxygen saturation does not have time to change. The problem of detecting and measuring changes in oxygen saturation on a continuous

time basis will be discussed in the next section.

It is reasonable to assume that as the flushed ear is being compressed, distortion of the bloodless ear by pressure will be a minimum at small pressures. Thus we should expect that the film of blood displaced from the vessels in the ear at small pressures would provide a more accurate determination of oxygen saturation than that quantity of blood displaced when the ear is highly compressed. In fact it is possible to compute oxygen saturation on a continuous basis as pressure is being applied by using the light measured on the uncompressed ear as an initial reading. At very low pressures the amount of blood displaced is small, and consequently measurements would be more susceptible to error from instrument limitations. At high pressures the instrument errors are smaller, but distortion of the bloodless ear will predominate and cause an inaccurate determination of the ratio R. There is some range of pressure, then, for which we might expect the highest accuracy in the oxygen saturation measurement. This behavior is illustrated in Fig. 4.1.

In the region of highest accuracy X should be reasonably independent of pressure. For experimental investigation purposes the curve of Fig. 4.1 may be computed with the ratio R (equation (3.23)) as the ordinate instead of X. If, during a test, it is possible to determine the region of highest accuracy with ease (i.e., visually), then this value of R may be associated with a simultaneously determined gasometric value of X to obtain a calibration curve

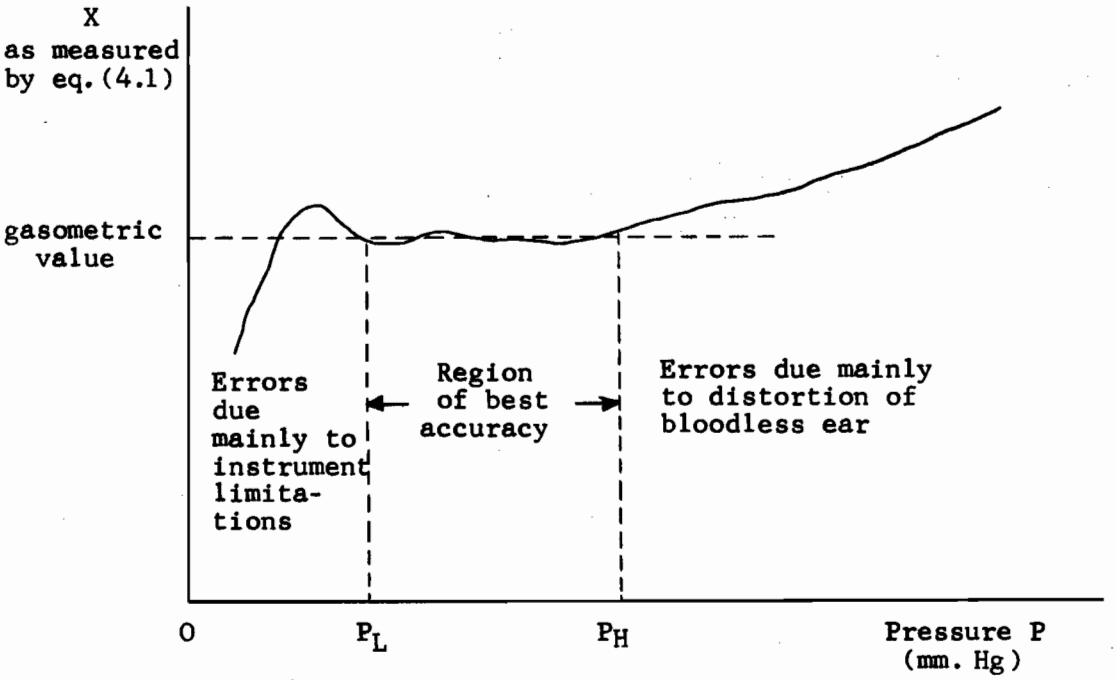

Fig. 4.1 Variation of measured oxygen saturation with pressure applied to the pinna. The initial readings in the red and infrared are determined at zero pressure. The Van Slyke determined value is also indicated and should coincide with that measured in the region of best accuracy.

for the instrument. If, on the other hand, there is no region of constant R that is well defined, other methods must be used to evaluate the optimum calibration curve, and also to determine that pressure range at which the highest accuracy in measuring X is most likely. In any event the results of studying a large number of such test curves should enlighten the knowledge of the effect of distortion in the bloodless ear.

For the case in which R is not reasonably constant over some range of pressure (this range of pressure should be reproducable

from ear to ear) we may proceed in the following manner to determine the optimum calibration curve. Suppose n experiments are performed in which curves of R vs. pressure as well as gasometric determinations are obtained. For each value of pressure we may compute the scatter of the points about the line of best fit on a calibration plot of R vs. the gasometric value of X. If we now plot the scatter against pressure we may arrive at that pressure range which is associated with the most probable value of oxygen saturation.

In practical use the earpiece would be fitted to the ear, readings made in the red and infrared, pressure of a pre-determined magnitude applied and final readings made on the partially compressed ear. Oxygen saturation is then easily computed from (4.1) since the constants have been pre-determined through calibration curves.

4.2 Continuous Measurement of Oxygen Saturation

Continuous time measurements of oxygen saturation are always less accurate than instantaneous ones for the following reason. In an instantaneous measurement we considered a film of blood introduced into a beam of light. As long as light readings were made before and after the insertion, oxygen saturation could be calculated. If, however, the initial light reading changed while the blood film was being inserted, then the calculated value of X would be in error. This same situation will occur if continuous measurements are attempted. If the initial light reading is to remain unchanged it is required that a true reading on the

bloodless ear be obtained, since any blood present in the ear when the measurement is made may change in oxygen saturation at a later time and thus effectively alter the initial reading.

The problem, then, becomes one of obtaining a suitable reading for the bloodless ear. It is obvious that any investigation must be experimental for each individual will have ears somewhat different from the next.

Let us consider a test which might aid in evaluating the readings taken on the fully compressed bloodless ear. Suppose that as the ear is being partially compressed we obtain an instantaneous measurement of oxygen saturation in accordance with the previous section. (We have assumed that the method outlined in section 4.1 is satisfactory and yields results of acceptable accuracy.) Call this value X_1. The ear is now fully compressed and readings are made in the red and infrared on the distorted "bloodless ear". The ear is allowed to become flushed once again and measurements are made on the complete cross-section including the blood. Let these latter readings be E_{r1} and E_{i1}. During this interval we assume that the value of the arterial oxygen saturation has not changed. Thus the best estimate of oxygen saturation is the instantaneous value, X_1, which is given by

$$X_1 = C_1 - C_2 \frac{\ln E_{r1} - \ln A}{\ln E_{i1} - \ln B} \tag{4.2}$$

where C_1 and C_2 are constants (previously determined) and A and B

are the <u>true</u> readings on the bloodless ear in the red and infrared, respectively, which may or may not correspond with the experimental values previously obtained.

The oxygen saturation of the subject is now changed to a new value, X_2, determined by another instantaneous measurement when the ear is again compressed. As before

$$X_2 = C_1 - C_2 \frac{\ln E_{r2} - \ln A}{\ln E_{i2} - \ln B} \tag{4.3}$$

where E_{r2} and E_{i2} are the readings in the red and infrared before the ear is compressed a second time. Assuming that the blood flow to the ear has not changed, then $E_{i1} = E_{i2} = E_i$. Solving (4.2) and (4.3) simultaneously for A and B yields

$$A = \frac{E_{r1}^{\left[\frac{X_2 - C_1}{X_2 - X_1}\right]}}{E_{r2}^{\left[\frac{X_1 - C_1}{X_2 - X_1}\right]}} \tag{4.4}$$

and

$$B = \left[\frac{E_{r1}}{E_{r2}}\right]^{\frac{C_2}{X_1 - X_2}} \tag{4.5}$$

Thus the readings on the bloodless ear may be calculated if X_1 and X_2 are sufficiently accurate. These "more accurate" bloodless ear readings may now be compared with the measured values obtained at

the start of the test to see if there is any characteristic point in the pressure vs. photocell output curves which, over many subjects, gives the best estimate of the true bloodless ear readings.

4.3 Experimental Evaluation

It should be emphasized at this point that the preceding discussion is not necessarily directly applicable to the design or operation of practical measuring equipment, but serves only as a basis for evaluating the maximum absolute accuracy of the ear oximeter technique. The experimental data required may be conveniently obtained from a small number of tests in the following manner. For each test curves are obtained in both the red and infrared bands of photocell current (or voltage) against pressure, which may be conveniently displayed on a two-pen X-Y recorder. In each case the pressure would be run sufficiently high so that the ear is fully compressed and all the blood excluded, except for that amount which is trapped regardless of how high the pressure is raised. Along with each set of curves a gasometric measurement of oxygen saturation would be obtained to serve as a standard for the test.

For analysis purposes the curves may be described numerically in a point-by-point manner and a digital computer used to statistically evaluate the relation discussed in sections 4.1 and 4.2. In this way the absolute accuracy of all phases of the technique may be investigated from a single set of curves for each test.

The best form of oximeter for clinical use will no doubt depend on the experimental evaluation of various systems. Instantaneous measurements might employ an analog computer to obtain the oxygen saturation X and display it as a function of pressure on an X - Y recorder. This visual display would indicate any irregularities in the determination and allow a better estimation of the true value of X from the "best estimate" section of the curve.

CHAPTER V

MODIFICATION OF EXISTING OXIMETER FOR CONTINUOUS RECORDING

An existing instrument for the measurement of oxygen saturation has been described by Sekelj. The operation and theory of this instrument differ slightly from that previously discussed and have been fully outlined in the American Heart Journal and other publications. Only a brief summary of the system will be given here along with the resulting modifications.

5.1 Existing Oximeter

The system consists of an earpiece, which contains the light source along with the appropriate filters and photocells, and electronic voltage amplifiers which provide sufficient gain to enable recorders and other instruments to be used. The earpiece itself is constructed so that different cross-sections of the ear are sampled in the red and infrared spectrums. Each cross-section is about 0.5 cm. in area. Gelatin filters are used in front of each iron-selenium photocell to select the proper light bands.

The main difference in this method is the assumption that the ratio of the true bloodless ear readings in the red and infrared is a constant, i.e. invariant from ear to ear. Thus if the initial light intensity distributions incident on the ear are $J'_{or}(\lambda,y,z)$ and $J'_{oi}(\lambda,y,z)$, and if we describe the bloodless ear

as an ideal light absorber (i.e. homogeneous tissue) so that its absorption coefficients are $\alpha_r(\lambda,y,z)$ and $\alpha_i(\lambda,y,z)$, then the following ratio is assumed constant:

$$\frac{k_r \int_A \int_\lambda G_r(\lambda)\, H_r(\lambda)\, J'_{or}(\lambda,y,z) \exp\left[-\alpha_r(\lambda,y,z)\, x_r(y,z)\right] d\lambda\, dA}{k_i \int_A \int_\lambda G_i(\lambda)\, H_i(\lambda)\, J'_{oi}(\lambda,y,z) \exp\left[-\alpha_i(\lambda,y,z)\, x_i(y,z)\right] d\lambda\, dA} = \text{const.} \tag{5.1}$$

where $x_r(y,z)$ and $x_i(y,z)$ are the depths of the bloodless ear in the red and infrared light paths respectively. Other parameters have been previously defined. If the absorption coefficients are functions of depth in the bloodless ear (as they probably are) the above relation must be modified accordingly.

5.2 Quantitative Evaluation of Oxygen Saturation

The expression for oxygen saturation is evaluated in much the same manner as that in Chapter II. The distributions with respect to wavelength and position are not considered. We define the following:

I_{or}	the red photocell output of the bloodless ear.
I_{oi}	the infrared photocell output of the bloodless ear. (It is not necessary to obtain these measurements if this method is employed.)
I_r	the red photocell output of the flushed ear.
I_{rs}	the red photocell output of the fully saturated (X = 1.0) flushed ear.
I_i	the infrared photocell output of the flushed ear.
ϵ_{1r}	the absorption coefficient of fully saturated blood in the red band.
ϵ_{or}	the absorption coefficient of fully reduced blood in the red band.

ϵ_i the absorption coefficient of blood in the infrared band.

d_1 the depth of fully oxygenated blood.

d_o the depth of fully reduced blood.

d the total depth of blood in the ear.

X the oxygen saturation of the blood.

K the ratio of the bloodless ear photocell outputs in the red and infrared bands. This is considered a constant for a particular earpiece.

The following relations must therefore apply (analogous to those in Chapter II):

$$I_r = I_{or} \exp\left[-(d_1\epsilon_{1r} + d_o\epsilon_{or})\right] \tag{5.2}$$

$$I_{rs} = I_{or} \exp\left[-d\epsilon_{1r}\right] \tag{5.3}$$

$$I_i = I_{oi} \exp\left[-d\epsilon_i\right] \tag{5.4}$$

$$d = d_1 + d_o \tag{5.5}$$

$$X = \frac{d_1}{d} \tag{5.6}$$

$$K = \frac{I_{or}}{I_{oi}} \tag{5.7}$$

The oxygen saturation may be algebraically determined from these relations, and is:

$$X = 1 - \frac{d_o}{d} \tag{5.8}$$

$$X = 1 - \frac{\epsilon_i - \epsilon_{1r}}{\epsilon_{or} - \epsilon_{1r}} \cdot \frac{\ln I_{rs} - \ln I_r}{\ln I_{rs} - \ln I_i - \ln K} \tag{5.9}$$

An empirical relation has been found to exist between I_{rs} and I_i, namely

$$I_{rs} = a(I_i - b) \log_{10} H \tag{5.10}$$

where a and b are constants for a particular earpiece and H is the hemoglobin concentration of the blood under test (gm/100 ml.). The value of H is determined from a venous blood sample. A simplification may be made since b is small and may be neglected. Thus (5.10) becomes:

$$I_{rs} = a I_i \log_{10} H \tag{5.11}$$

Combining equations (5.9) and (5.11) and defining

$$H_L = \log_{10} H \tag{5.12}$$

and

$$C = \frac{\epsilon_i - \epsilon_{1r}}{\epsilon_{or} - \epsilon_{1r}} > 0 \tag{5.13}$$

yields

$$X = 1 - C + \frac{C}{\ln \frac{aH_L}{K}} (\ln I_r - \ln I_i - \ln K) \tag{5.14}$$

The experimental calibration curve arising from a plot of the gasometric determination, X, vs. the measured ratio $(\ln I_{rs} - \ln I_r)/(\ln I_{rs} - \ln I_i - \ln K)$ results in a non-linear relation (Fig. 5.1). This may be approximated by a straight line with an ordinate intercept of X_o. Thus equation (5.14) must be modified

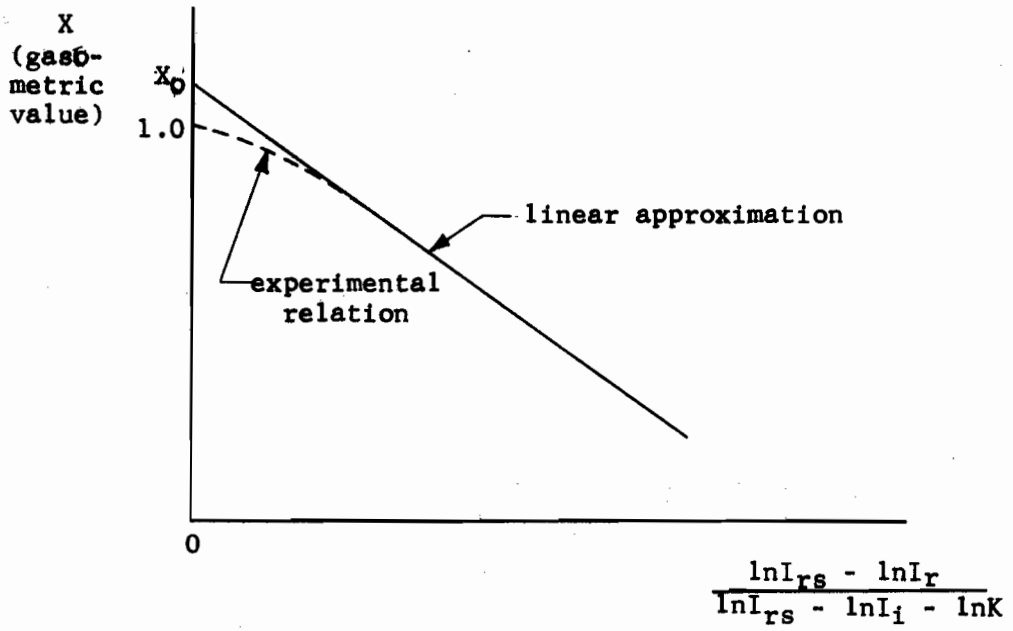

Fig. 5.1 Linear Approximation to experimental oximeter calibration curve.

to include X_o as the intercept rather than the theoretically calculated value of 1.0 in equation (5.9). This results in

$$X = B + \frac{C}{\ln \frac{aH_L}{K}} (\ln I_r - \ln I_i - \ln K) \qquad (5.15)$$

where

$$B = X_o - C \qquad (5.16)$$

The expression (5.15) for X is easily evaluated as follows: assume the constants B, C, a, and K have previously been determined from the calibration curves (Fig. 5.1 and equation (5.10)) and that H is known from a blood test. The earpiece is now placed on the subject's ear and I_r and I_i are read. X is then calculated

from (5.15). It should be noted that before the earpiece is placed on the ear the outputs of the photocells are adjusted to pre-determined values with a standardizing filter in place. The gains of the amplifiers must then remain constant throughout the experiment.

Consider the amplification of the signals. Let

$$E_r = \alpha I_r \tag{5.17}$$

and

$$E_i = \beta I_i \tag{5.18}$$

so that equation (5.14) becomes

$$X = B + \frac{C}{\ln\frac{aH_L}{K}}\left[\ln E_r - \ln E_i - \ln(K\frac{\alpha}{\beta})\right] \tag{5.19}$$

If the base of the logarithm is changed from e to b then

$$\ln x = \ln b \, \log_b x \tag{5.20}$$

and

$$X = B + \frac{C \ln b}{\ln\frac{aH_L}{K}}\left[\log_b E_r - \log_b E_i - \log_b(K\frac{\alpha}{\beta})\right] \tag{5.21}$$

$$= B + A\left[D + \log_b E_r - \log_b E_i\right] \tag{5.22}$$

where

$$A = \frac{C \ln b}{\ln\frac{aH_L}{K}} \tag{5.23}$$

and

$$D = -\log_b \left(K\frac{\alpha}{\beta}\right) \tag{5.24}$$

Equation (5.22) is now in a form convenient for electronic analog computation and a block diagram of the setup is shown in Fig. 5.2. Three operational amplifiers and two logarithmic function generators are employed.

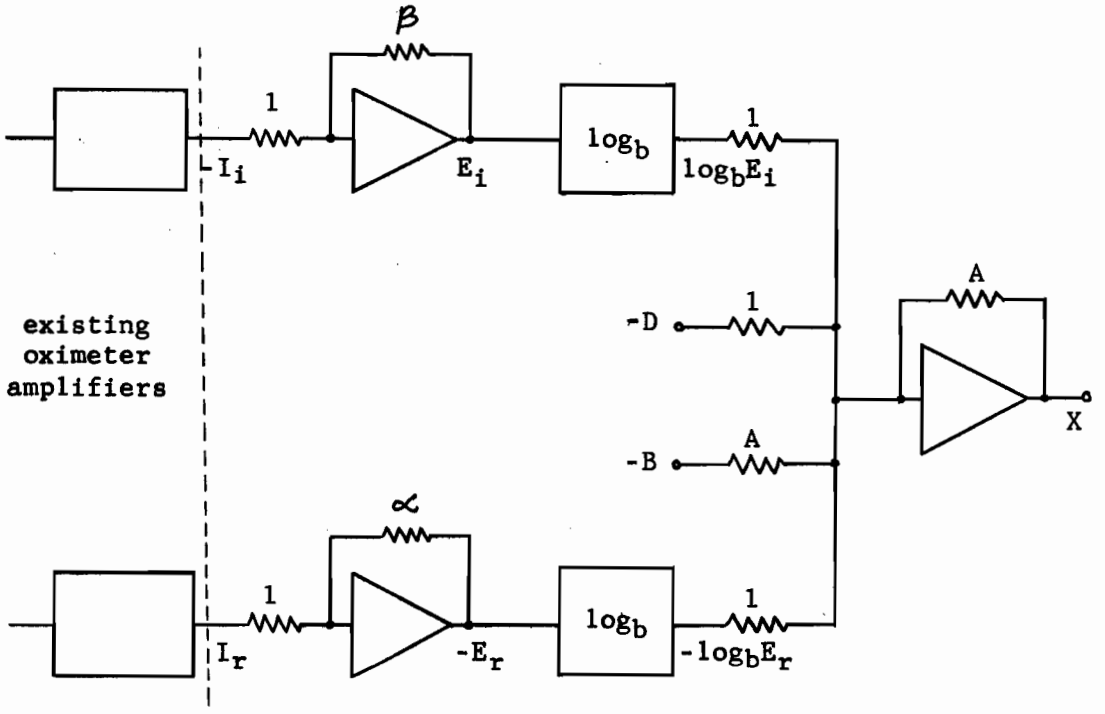

$$X = B + A\left[D + \log_b E_r - \log_b E_i\right]$$

Fig. 5.2 Block diagram of simple analog computer for oximeter.

5.3 Logarithmic Function Generators

Since the accuracy of the computing system depends to a large extent on the log function generators these will be

discussed in detail. The most efficient use of equipment results if the log generators are employed at the outputs of the two amplifiers in the red and infrared channels. A diode network is used as a voltage divider to approximate the function, as illustrated in Fig. 5.3.

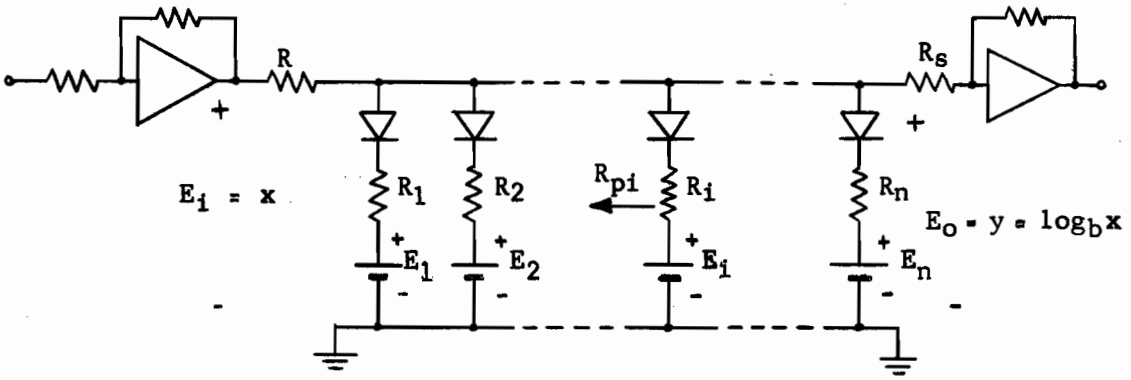

Fig. 5.3 Diode network used to obtain a piecewise linear approximation to a logarithmic curve.

The first consideration is the choice of the logarithmic base b. Since the output voltage of the log network can never be greater than the input voltage the choice of b is restricted. To improve accuracy we would, however, like the change in the output voltage to be as large as possible for a change in input voltage. Fig. 5.4 shows the log curve and its straight line approximation.

The limiting value of b may be determined as follows: the log curve is described by

$$y = \log_b x \tag{5.25}$$

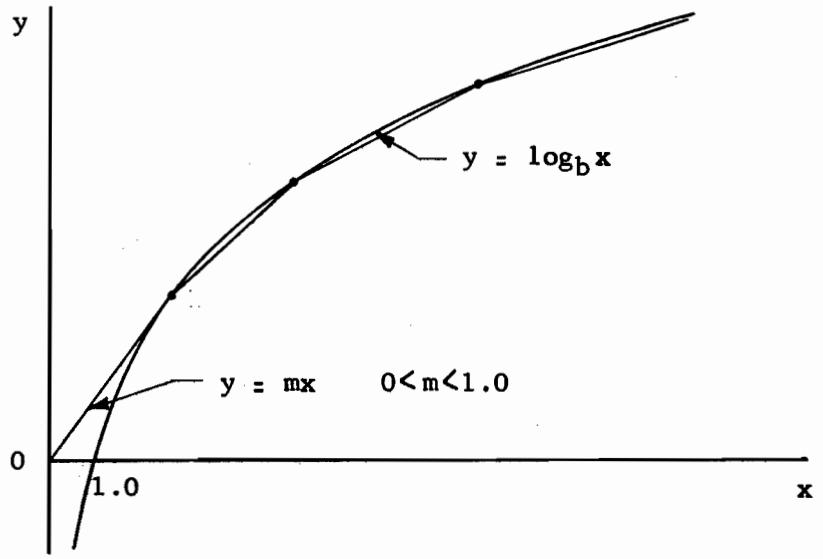

Fig. 5.4 Straight line approximation to curve $y = \log_b x$.

and the first straight line segment by

$$y = mx \tag{5.26}$$

A simultaneous solution for the tangent point P yields

$$mx = \log_b x = \frac{\ln x}{\ln b} \tag{5.27}$$

therefore

$$\ln b = \frac{\ln x}{mx} \tag{5.28}$$

At this tangent point the slopes of the curves must be equal, i.e.

$$m = \frac{1}{x \ln b} \tag{5.29}$$

and thus

$$\ln b = \ln x \ln b \tag{5.30}$$

for which x = 2.718 regardless of the base b. Thus if we restrict m to values $0 < m < 1.0$ and consider m = 1.0 as a limiting value, b may be found from (5.28), viz

$$\ln b = \frac{\ln (2.718)}{(1.0)(2.718)} \tag{5.31}$$

which gives

$$b = 1.445 \tag{5.32}$$

To include a safety factor for diode leakage b was chosen as 1.5.

The breakpoint co-ordinates (x_i, y_i) were chosen on an absolute error basis and this is shown in Fig. 5.5 where Δy is the error between the straight line segment and the curve $y_c = \log_b x$.

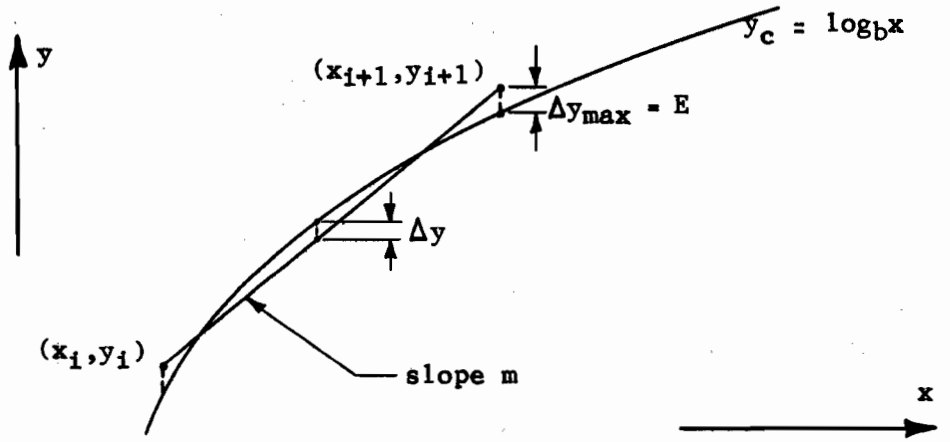

Fig. 5.5 Straight line approximation to logarithmic curve showing the error of approximation.

The maximum error is $\Delta y_{max} = E$. We may write the equation for the straight line as

$$y = y_i + m(x - x_i) \tag{5.33}$$

and that for the curve as

$$y_c = \log_b x \tag{5.34}$$

$$= \frac{\ln x}{\beta} \tag{5.35}$$

where

$$\beta = \ln b \tag{5.36}$$

Now

$$\Delta y = y_c - y \tag{5.37}$$

$$= \frac{\ln x}{\beta} - y_i - m(x - x_i) \tag{5.38}$$

Δy is a maximum when

$$\frac{d(\Delta y)}{dx} = 0 \tag{5.39}$$

or

$$x = \frac{1}{m\beta} \tag{5.40}$$

therefore

$$\Delta y_{max} = E = \frac{\ln(\frac{1}{m\beta})}{\beta} - y_i - \frac{1}{\beta} - mx_i \tag{5.41}$$

so that

$$m = \frac{1}{\beta x_i}\ (1 + \beta E + \beta y_i) - \ln(\frac{1}{\beta m}) \tag{5.42}$$

Since

$$E = y_{i+1} - y_c\Big|_{x = x_{i+1}} \tag{5.43}$$

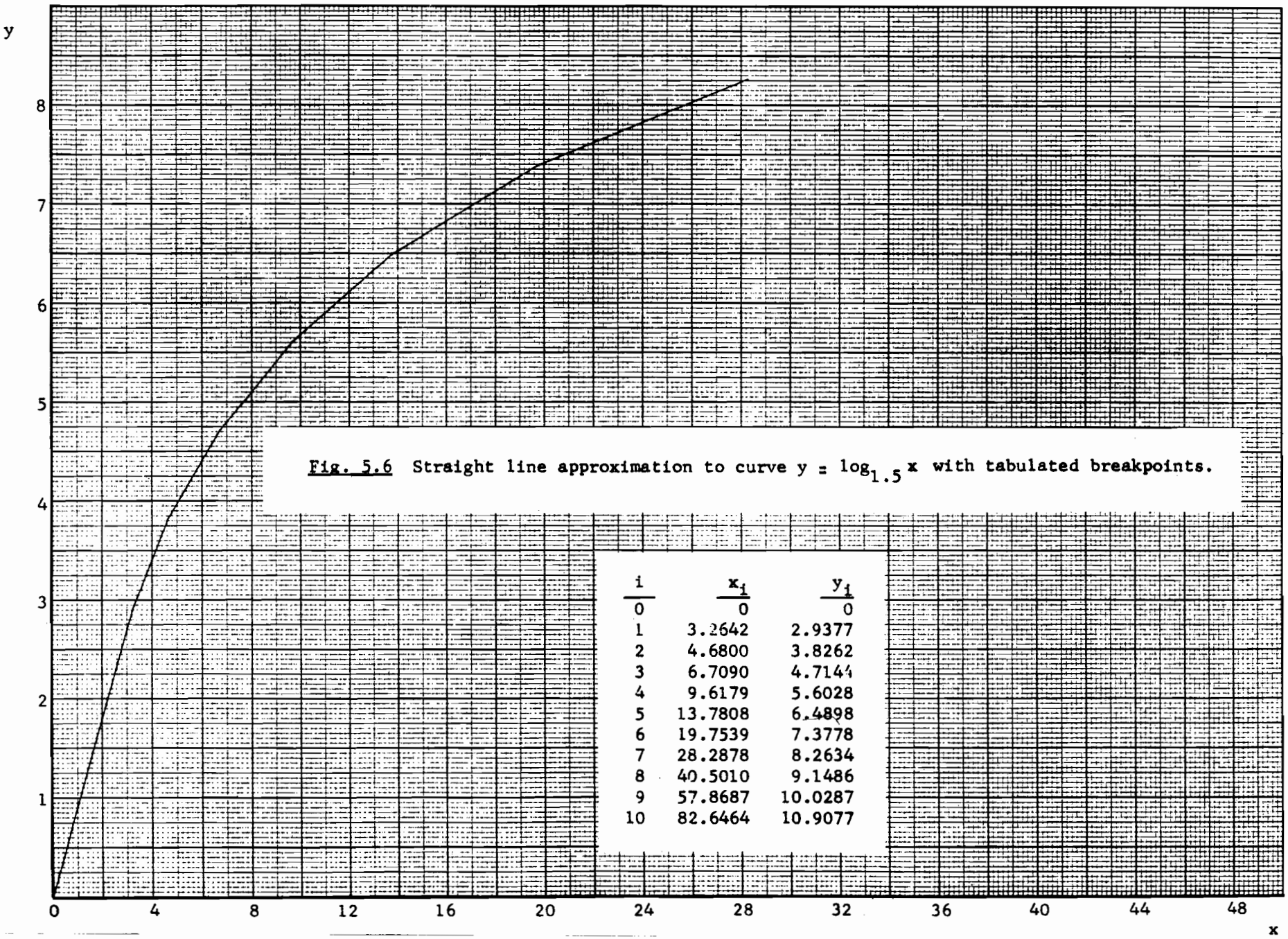

Fig. 5.6 Straight line approximation to curve $y = \log_{1.5} x$ with tabulated breakpoints.

i	x_i	y_i
0	0	0
1	3.2642	2.9377
2	4.6800	3.8262
3	6.7090	4.7144
4	9.6179	5.6028
5	13.7808	6.4898
6	19.7539	7.3778
7	28.2878	8.2634
8	40.5010	9.1486
9	57.8687	10.0287
10	82.6464	10.9077

$$E = y_i + m(x_{i+1} - x_i) - \frac{\ln x_{i+1}}{\beta} \tag{5.44}$$

we may solve for x_{i+1} to give

$$x_{i+1} = \frac{1}{m\beta}\left[\beta(E + mx_i - y_i) + \ln x_{i+1}\right] \tag{5.45}$$

thus

$$y_{i+1} = y_i + m(x_{i+1} - x_i) \tag{5.46}$$

A numerical solution for all breakpoints was obtained on an IBM 1410 digital computer using iterative techniques and equations (5.42), (5.45), and (5.46). The first breakpoint (x_1, y_1) is obtained by setting $x_i = y_i = 0$, in which case

$$m = \frac{1}{\beta \exp(1+\beta E)} \tag{5.47}$$

Fig. 5.6 shows the straight line approximation for the following values: b = 1,5, E = 0.02.

The log network components are now obtained in the following manner. If we consider the i^{th} section of the network shown in Fig. 5.3 we may express the parallel resistance looking back into the (i - 1) sections as

$$R_{pi} = \frac{1}{G_{pi}} \tag{5.48}$$

where

$$G_{pi} = G_s + \sum_{j=1}^{i-1} G_j \tag{5.49}$$

The G's are the conductances of the resistive elements with the same subscripts. The slope of the i^{th} section is given by

$$m_i = \frac{y_{i+1} - y_i}{x_{i+1} - x_i} \tag{5.50}$$

$$= \frac{R_i \| R_{pi}}{R + R_i \| R_{pi}} \tag{5.51}$$

Solving for R_i yields

$$R_i = \frac{R_{pi}\, m_i}{R_{pi}(1 - m_i) - m_i R} \tag{5.52}$$

thus if R_1, R_2 .... R_{i-1} and m_i are known, R_i may be calculated. For the first section R_s is specified and R is determined from

$$R = \left(\frac{x_1}{y_1} - 1\right) R_s \tag{5.53}$$

The breakpoint voltages E_i are found from

$$E_i = y_i - V \tag{5.54}$$

where V is the approximate forward breakpoint voltage of the silicon diodes used. These calculations are convenient for processing by digital computer.

The network illustrated in Fig. 5.7 results when R_s = 1 Megohm and V = 0.35 v. The breakpoints are those calculated and

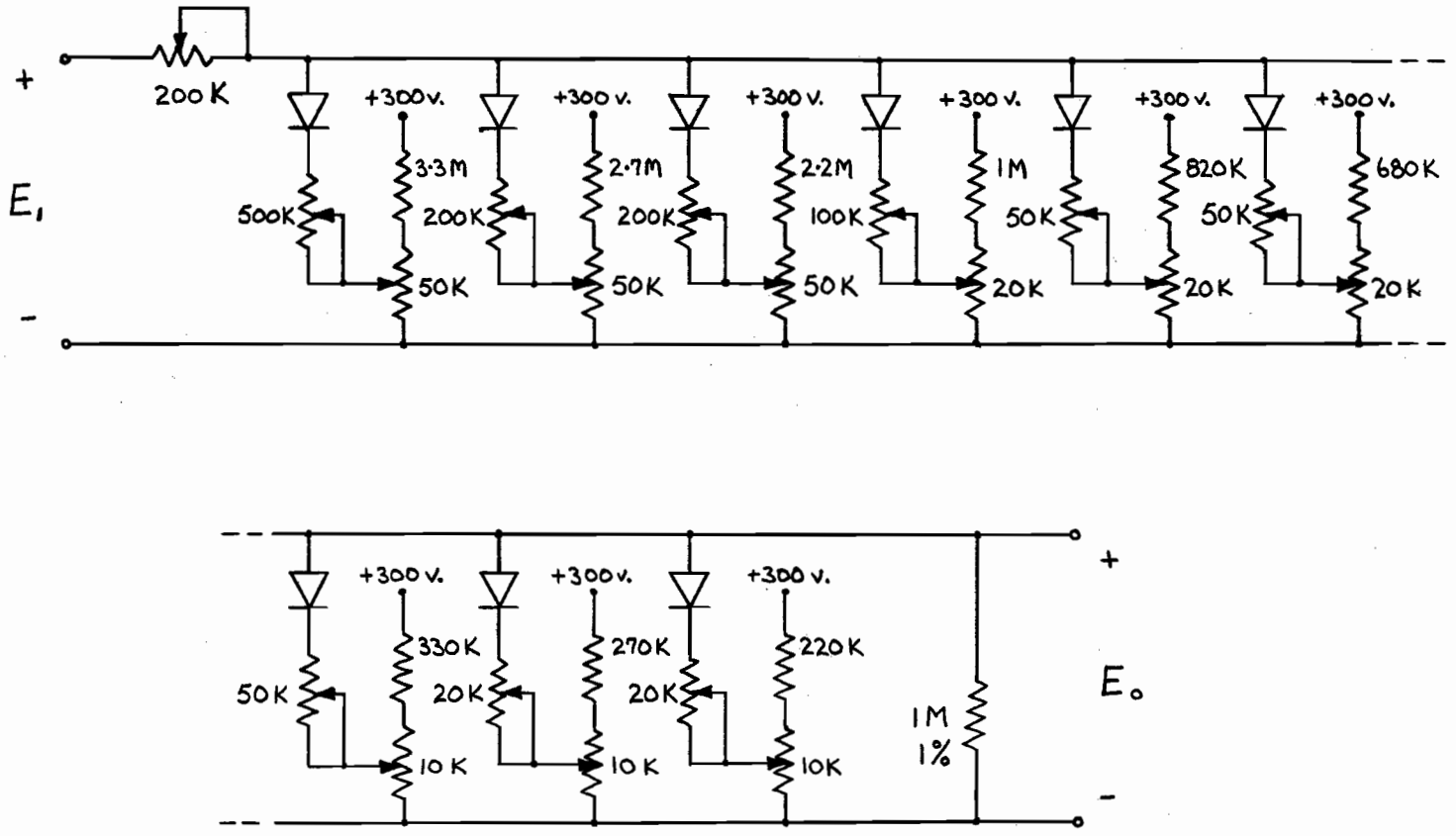

Fig. 5.7 Logarithmic Function Generator. When properly aligned $E_o = \log_{1.5} E_i$ ($2 < E_i < 100$ v.) to within an error of $\pm$ 0.02 v. in E_o. All resistors are ½ watt and the diodes are silicon.

shown in Fig. 5.6. A step-by-step alignment is finally required to calibrate the log generator.

5.4 Analysis of Computer Accuracy

The overall accuracy of the computer is independent of the initial component tolerances once the log networks have been calibrated. Errors will arise due to changes in temperature, power supply voltage, amplifier drift, and any drift in the existing oximeter associated with the earpiece. The high voltage power supply employed is rated at 300 v. ± 0.033% at 100 ma. maximum and this drift was considered sufficiently small to be neglected. For this reason the power supply was also used as a reference bias source for the diodes in the log network.

A block schematic of the computer is shown in Fig. 5.8. The input voltages from the existing oximeter are denoted by $I_i + \Delta I_i$ and $I_r + \Delta I_r$, where ΔI_i and ΔI_r are the drift errors associated with the oximeter. If we let the long term operational amplifier drifts referred to the input be δ_a volts, and the error associated with the log networks be δ_L volts, the output of the computer is

$$X = B + A\left[D + \log_{1.5}\left\{\alpha(I_r + \Delta I_r) + \alpha\delta_a\right\} + \delta_L - \log_{1.5}\left\{\beta(I_i + \Delta I_i) + \beta\delta_a\right\} + \delta_L\right] \qquad (5.55)$$

Also since $E_r = \alpha I_r$ and $E_i = \beta I_i$ we have from (5.55)

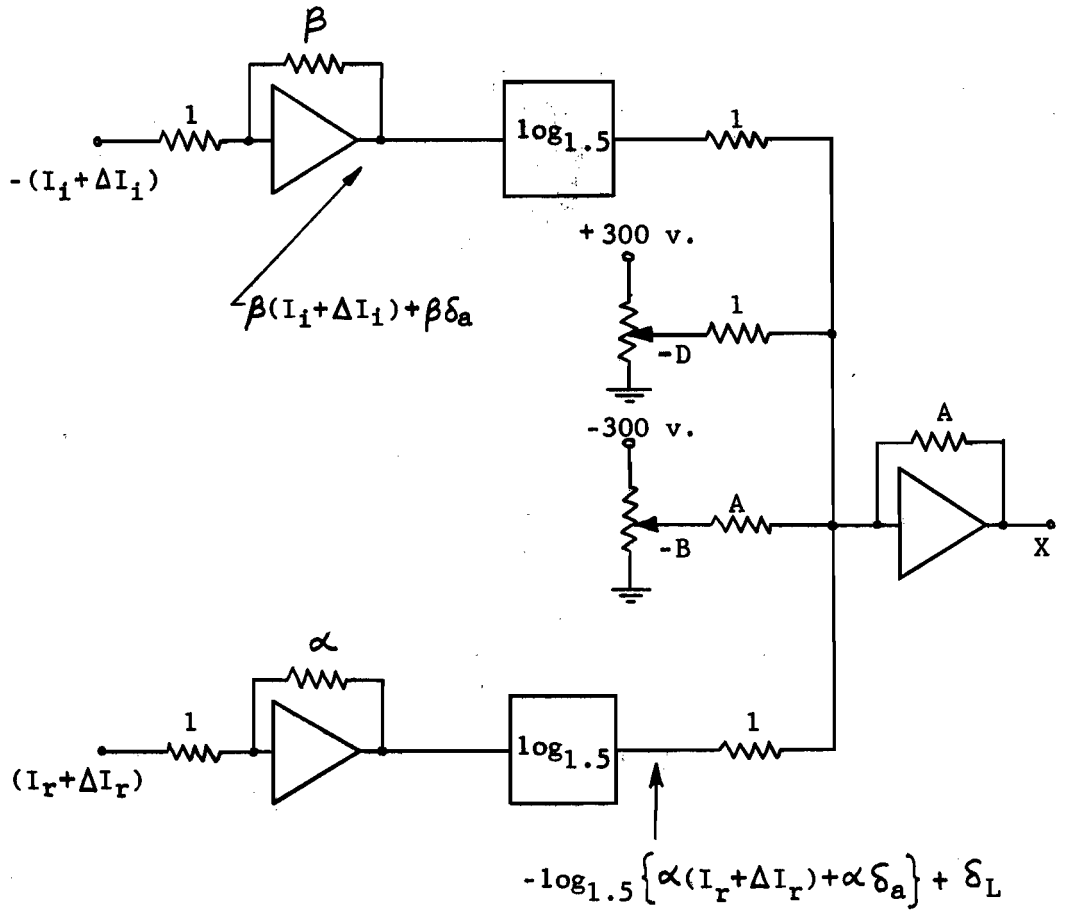

Fig. 5.8 Block schematic of computer showing the accumulation of errors.

$$X = B + A\left[D + \log_{1.5} E_r - \log_{1.5} E_i\right] + \delta \qquad (5.56)$$

where the error in oxygen saturation is δ, which for the worst case (all errors additive) is less than

$$2A\delta_L + \frac{A}{\ln 1.5}\left[\frac{\alpha\delta a}{E_r} + \frac{\beta\delta a}{E_i}\right] + \frac{A}{\ln 1.5}\left[\frac{\Delta I_r}{I_r} + \frac{\Delta I_i}{I_i}\right] \qquad (5.57)$$

The first two terms refer to the error due only to the computer itself. The worst case occurs for the following values:

$$\begin{aligned} A &= 0.4 \\ \delta_L &= 0.02 \text{ v.} \\ \alpha &= \beta = 100 \\ E_r &= E_i = 5 \text{ v.} \end{aligned} \tag{5.58}$$

Thus

$$\delta < 0.016 + 0.004 + \left[\frac{\Delta I_r}{I_r} + \frac{\Delta I_i}{I_i}\right] \tag{5.59}$$

$$= 0.02 + \left[\frac{\Delta I_r}{I_r} + \frac{\Delta I_i}{I_i}\right] \tag{5.60}$$

The maximum error for the computer is thus less than ± 2% in the calculated oxygen saturation X, of which the major contribution comes from the log networks. An improvement in accuracy may be obtained if the log function generators are made more precise by selecting a smaller design error. Two per cent was considered sufficient for clinical use. It should be noted that a considerable error may occur from drift in equipment associated with the earpiece as the per cent drift in each channel is essentially added to the possible error in X. The only way this can be minimized is by the use of stable and drift free amplifiers.

5.5 Computer Performance

A schematic circuit diagram of the completed computer is shown in Fig. 5.9. Before the performance of the computer can

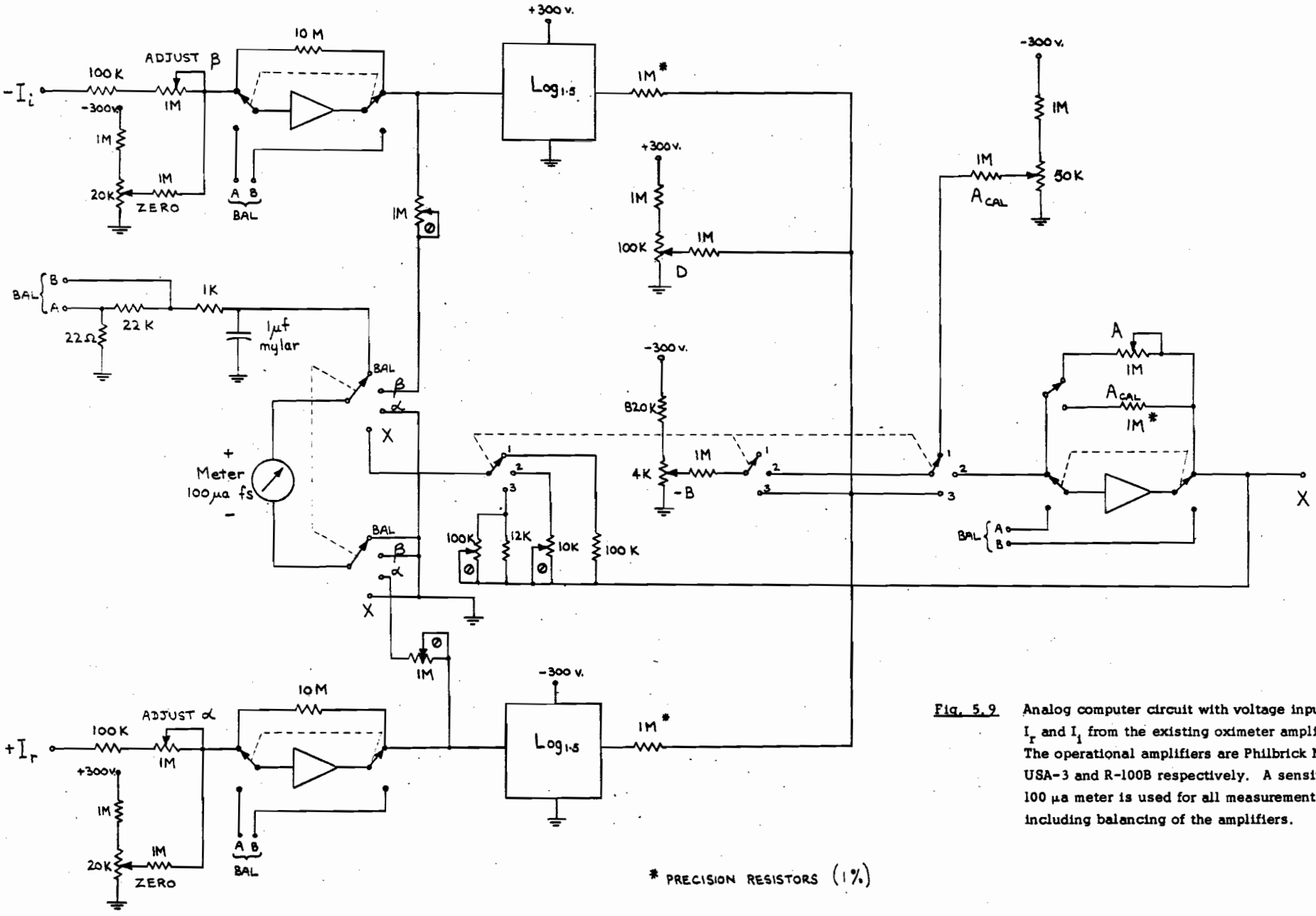

Fig. 5.9 Analog computer circuit with voltage inputs I_r and I_l from the existing oximeter amplifiers. The operational amplifiers are Philbrick Nos. USA-3 and R-100B respectively. A sensitive 100 μa meter is used for all measurements including balancing of the amplifiers.

be assessed it must be calibrated with respect to supply voltage and the log function networks. The Philbrick power supply used was found to have a drift of less than ± 100 mv. from its set value of 300 volts, which was within the manufacturer's specifications. The log function generators were next aligned by trimming the potentiometers in the network of Fig. 5.7. It was found that the most convenient and accurate method of aligning the diode networks was to use a dry pen X - Y plotter with the straight line segments of the log curve approximation pre-drawn on the co-ordinate paper. The static accuracy of the recorder used was rated at ± 0.15% of full scale which, on the ten volt range, gave a maximum error of 0.015 volts. This was considered adequate for initial test purposes since the design accuracy of the log networks is ± 0.02 v. The alignment procedure itself, after the equipment had been set up and calibrated, required less than five minutes. The resulting log function generators were matched to within a visible accuracy of 0.01 volts, and the experimentally recorded curve is illustrated in Fig. 5.10.

Since the diode breakpoints are rounded and not abrupt the curves are quite smooth, and it should be possible with accurate measuring equipment to improve on the ± 0.02 v. maximum design error. This was one of the reasons why more diodes were not used to achieve a higher accuracy in approximating the curve.

With the calibration of the oximeter complete, tests were made using filters to simulate ears of various oxygen saturations.

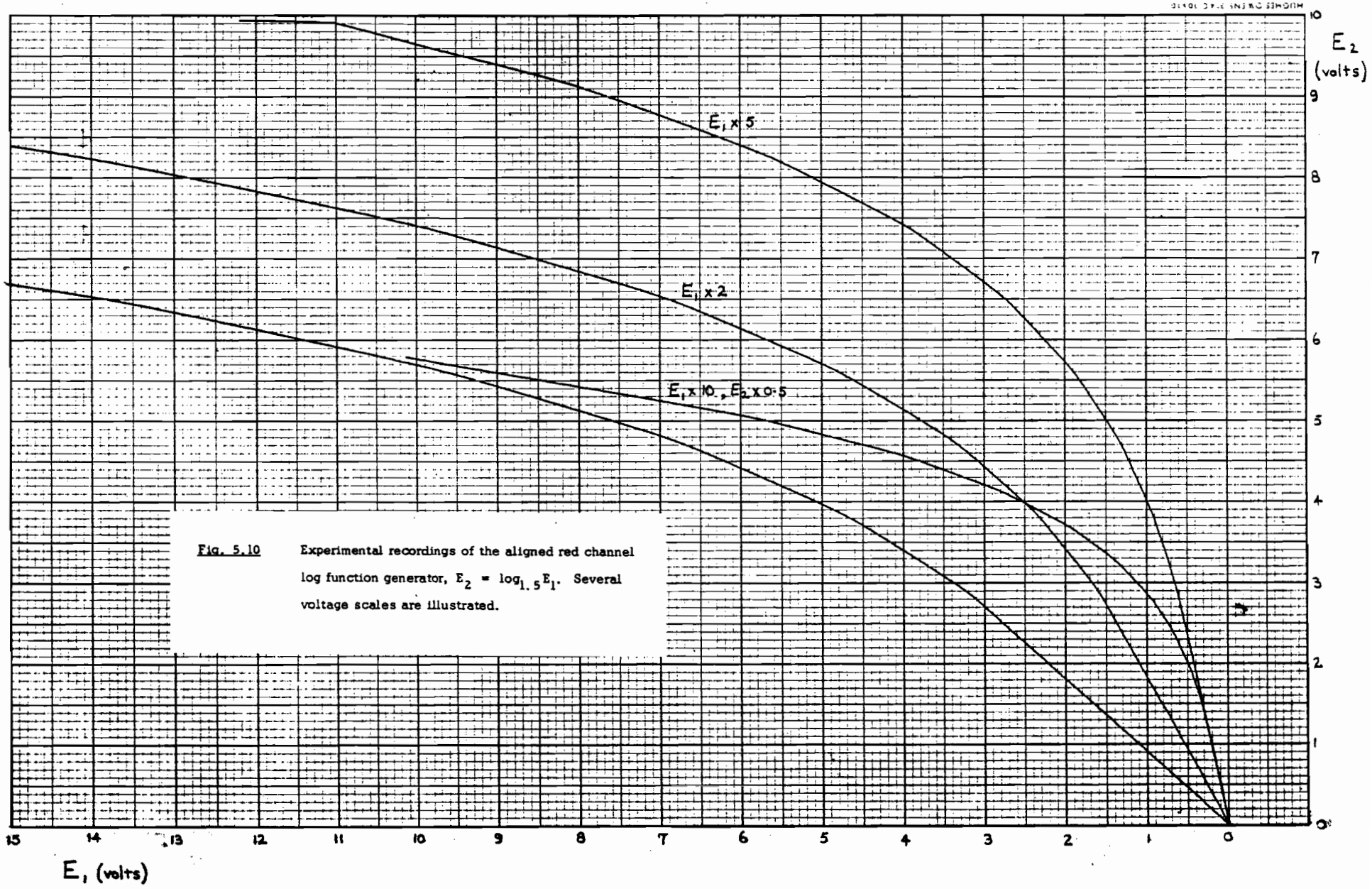

Fig. 5.10 Experimental recordings of the aligned red channel log function generator, $E_2 = \log_{1.5} E_1$. Several voltage scales are illustrated.

The electronically computed value was compared with the value manually calculated from equation (5.15) and the outputs of the existing oximeter. Three filters were used, each of which had different optical densities in the red and infrared bands thus simulating three different oxygen saturations for an assumed hemoglobin concentration of 14 gm/100 ml. The first filter (A) was used as a standard for calibration of both the computer and oximeter, while filters B and C were used to provide checks on the outputs in each channel and on oxygen saturation. With the oximeter and computer carefully calibrated the results shown in Table 5.1 were obtained.

Filter	Existing Oximeter X manually calculated			Electronic Computer X electronically computed		
	I_r	I_i	X%	E_r	E_i	X%
A (standard)	54.7	27.0	101.0	98.0	64.0	101.0
B	41.5	23.5	86.0	75.0	55.5	86.5
C	28.5	16.2	85.0	51.6	38.8	84.5

Table 5.1

The calculation of X for filter B was made with the following values (constants of the existing oximeter except for B): B = 1.0, C = 0.6625, a = 1.75, H = 14, K = 1.0. Thus from (5.15)

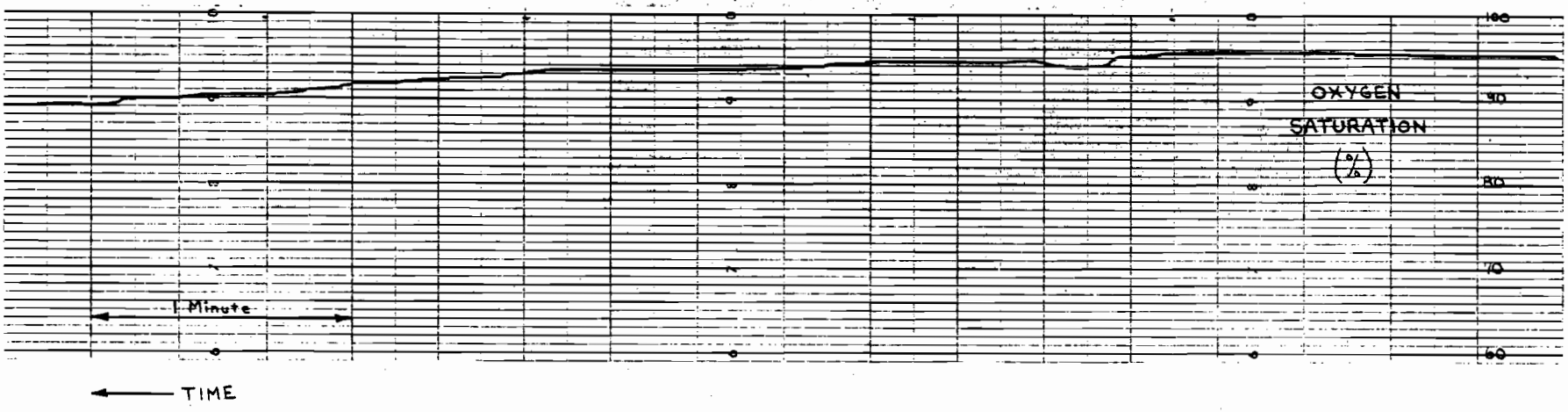

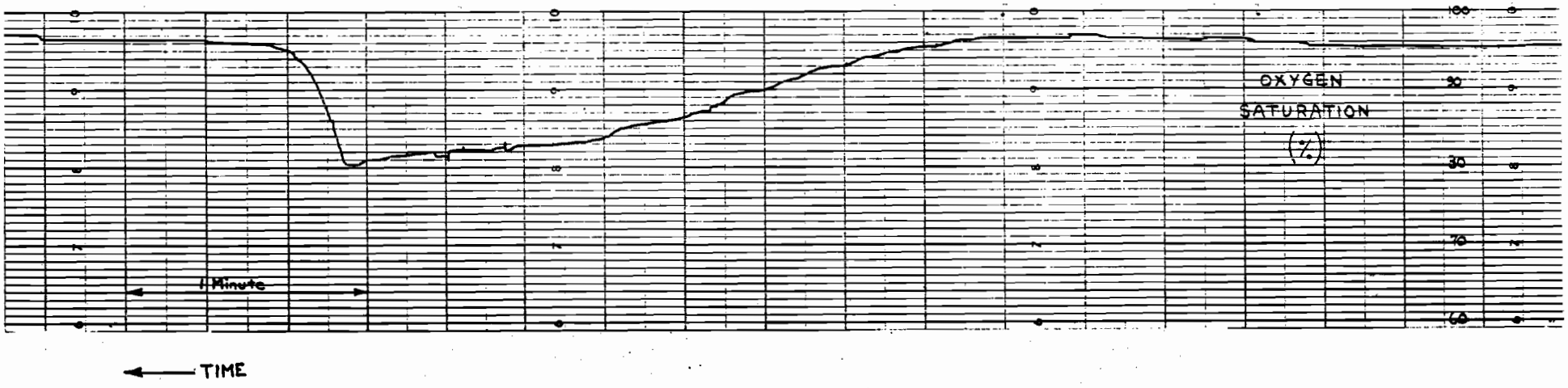

Fig. 5.11 A

Continuous time recordings of oxygen saturation. In the upper curve the subject was initially breathing air at A. A 16% oxygen (84% nitrogen) mixture was administered at B and a 12% mixture at C. In the lower curve the subject was initially breathing air at A. Pure oxygen was administered at B and a low oxygen mixture at C. Air breathing was resumed at D.

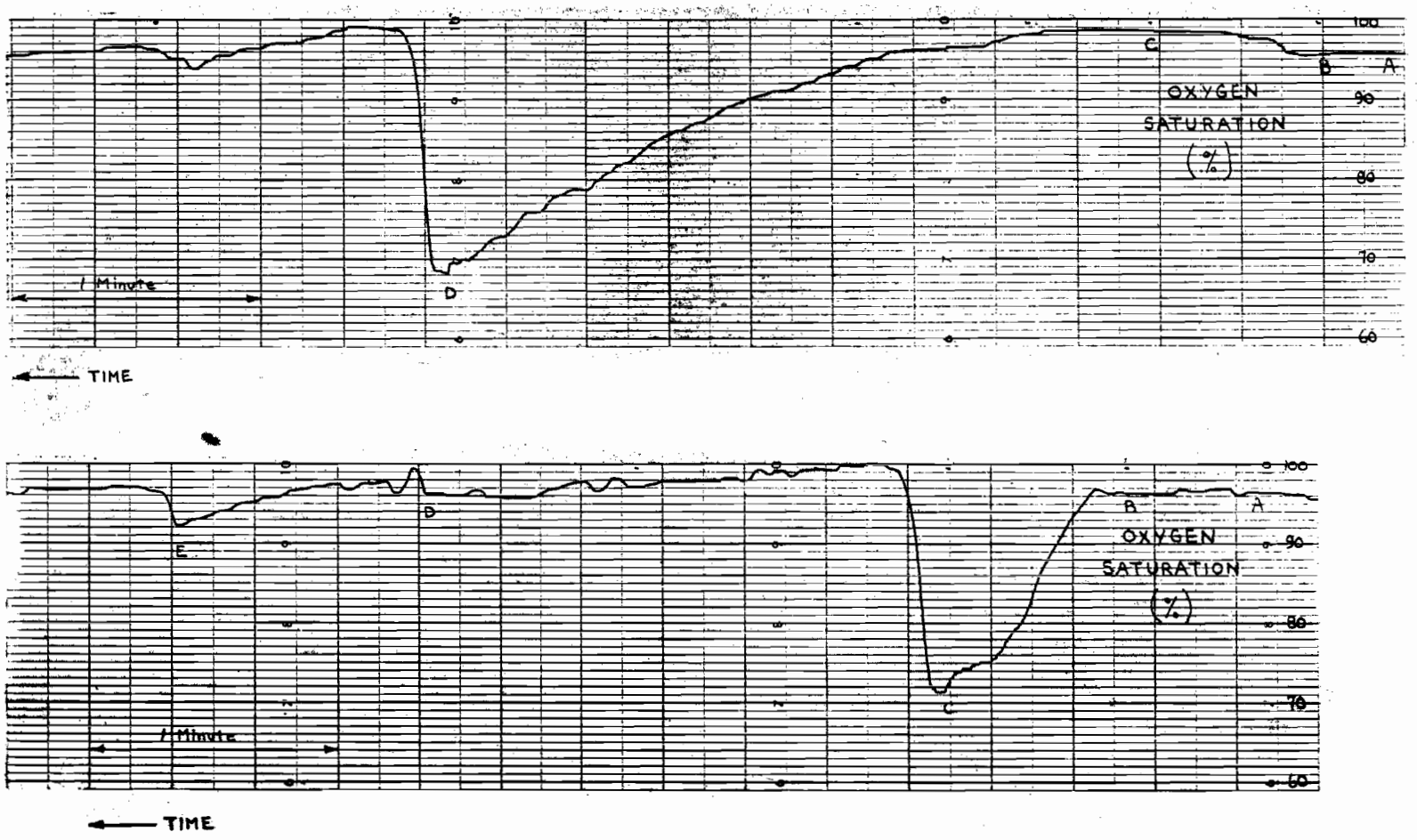

Fig. 5.11 B Continuous time recordings of oxygen saturation during breath-holding. In the upper curve the subject was initially breathing air at A, commenced hyperventilation at B, held a deep breath at C, and resumed breathing air at D. In the lower curve the subject was initially breathing air at A, performed a deep expiration at B, and resumed breathing air at C. A Val Salva manoeuvre was performed at D, followed immediately by breath-holding which ended at E.

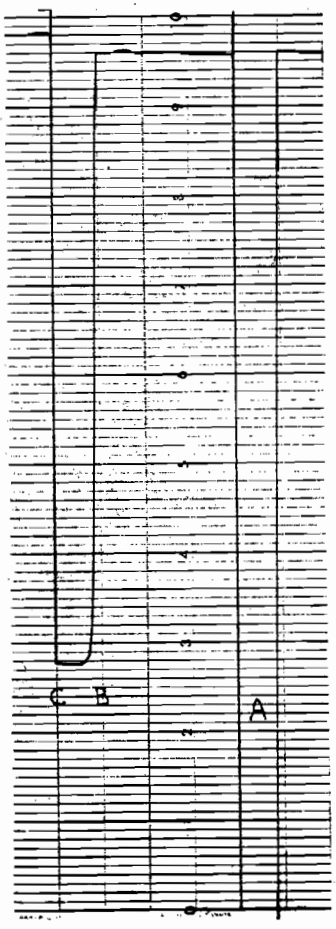

Fig. 5.11 C Step response of recorder alone at A, and of the complete system when the light was suddenly turned off at B and on at C. The time scale is the same as in Figs. 5.11 A and B.

$$X = 1.0 + \frac{0.6625}{\log \frac{1.75 \log 14}{1.0}} (\log 41.5 - \log 23.5 - \log 1.0)$$

$$= 0.8585$$

$$= 86.0\% \qquad (5.61)$$

In all cases where the system was accurately aligned the electronically computed values were within two per cent of those manually calculated. Drift in the computer was negligible and the output remained within ± 2% of the initial value, these changes being due to a slight drift in the existing oximeter amplifiers.

Several tests were made on a continuous time basis with the subject breathing various mixtures of air and nitrogen. These are illustrated in Fig. 5.11 A. Other experiments involving breath-holding were carried out and the results are shown in Fig. 5.11 B. Fig. 5.11 C gives an indication of the step response of the recorder alone and the system as a whole when the light source was suddenly switched off. The overall system rise time is in the order of 1.5 seconds.

CHAPTER VI

CONCLUSIONS

The analysis carried out in Chapters I, II and III attempts to explain some of the errors which have been present in ear oximetry measurements since the method was initiated by Millikan in 1942. These errors arise from non-uniform blood depth distributions, non-uniform light intensity distributions, non-monochromatic light measurements, and the sampling of two different cross-sections of the pinna in the red and infrared light bands. Experimental verification of these results has been found in the literature over the past two decades, and essentially the same behavior has been obtained by many independent investigators. It is unfortunate that these errors do not lend themselves to correction -- in fact it is difficult to estimate the relative magnitude of some of these effects without performing many experiments, and even then it is doubtful if an accurate estimation could be made. We do not need to know the relative magnitudes, however, since the study indicates the proper steps to take in order to eliminate or minimize these errors in a practical oximeter.

Another potential source of error is the effect of light scattering, which has been mentioned only. Its exact behavior is not fully known or understood even in cuvettes, and until an oximeter is developed to minimize the errors previously outlined it is doubtful if any experimental evidence concerning its effects in the ear

could be obtained.

The concept of the "bloodless" ear in deriving the equations of ear oximetry is necessary and of course only truly valid if the ear is considered ideal. As yet the effect of the "bloodless" ear on oxygen saturation measurements has not been fully assessed since published data concerns ears pressurized above systolic value in an attempt to remove all the blood. It is hoped that the method and approach suggested in Chapter IV will be of help in evaluating the effect of compressing the ear as a source of error in the use of oximeters. The method used by Sekelj could also be evaluated by the data obtained in the same test.

The computer outlined in Chapter V was constructed for use with an existing Sekelj oximeter. Its performance is within the designed accuracy although the resulting output is a linear relation rather than the experimental curve illustrated in Fig. 5.1. To compute the exact experimental relation it is necessary to add a correcting diode function generator to the output of the summing amplifier in the same manner as the diode log networks were employed. Such a network has not yet been incorporated into the computer just described.

From a clinical viewpoint the use of ear oximetry as a technique for obtaining and monitoring the oxygen saturation of arterial blood is highly desirable. It is evident that there will always be some uncertainty in readings obtained by this method, but it appears that the absolute accuracy of the technique itself can

now be evaluated. From this evaluation the design of a clinical instrument should take the following points into consideration. A first requirement is that the accuracy and consistency of the determination be acceptable. Secondly, the instrument must be stable and simple to use, preferably by untrained personnel. To be fully effective it should also be easily portable.

APPENDIX I

LIGHT AND PHOTOCELL RESPONSE

From energy considerations of light falling on a black body one may obtain the power density spectrum at a point, $J(\lambda)$ (watts/m^2/unit wavelength), as shown below.

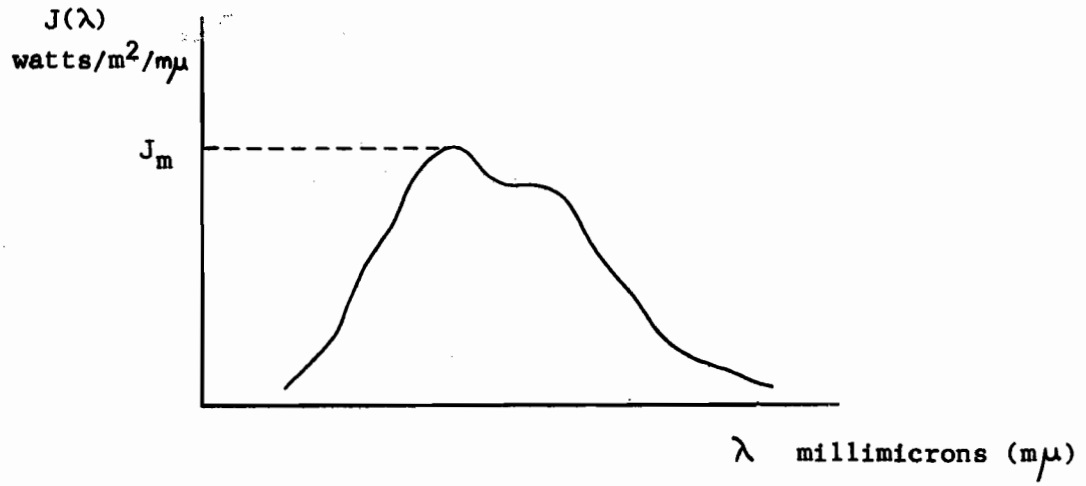

This may be expressed as

$$J(\lambda) = J_m\, j(\lambda)$$

where $j(\lambda)$ is the normalized response. In general the power density spectrum may be a function of position (y,z) over an area A(y,z) under consideration. Thus we may express the power density as

$$J(\lambda,y,z) = J_m\, j(\lambda,y,z)$$

where $j(\lambda,y,z)$ is the normalized response with respect to position and wavelength. The total radiant power available over the area A

is

$$W_p = \int_A \int_\lambda J(\lambda,y,z)\, d\lambda\, dA$$

$$= J_m \int_A \int_\lambda j(\lambda,y,z)\, d\lambda\, dA$$

If a photocell with a relative response $H(\lambda,y,z)$ intercepts this light then its short circuit current in the linear range is given by

$$i = k \int_A \int_\lambda H(\lambda,y,z)\, J(\lambda,y,z)\, d\lambda\, dA$$

where k is a constant. In terms of the total radiant power available

$$i = k W_p \frac{\int_A \int_\lambda H(\lambda,y,z)\, j(\lambda,y,z)\, d\lambda\, dA}{\int_A \int_\lambda j(\lambda,y,z)\, d\lambda\, dA}$$

$$= k W_p \left[\underline{\text{Relative Effectiveness}} \text{ of Photocell} \right]$$

In practical measurements with photocells one usually assumes a constant characteristic response over their surface. Also, the spectral distribution of the incident light is independent of position and constant in magnitude over the area covered by the cell. Under these conditions:

$$J(\lambda,y,z) = J(\lambda) = J_m\, j(\lambda)$$

and

$$H(\lambda,y,z) = H(\lambda)$$

The radiant power density (watts/m^2) over the surface is therefore

$$W = \int_\lambda J(\lambda)\, d\lambda$$

$$= J_m \int_\lambda j(\lambda)\, d\lambda$$

The photocell current is

$$i = k \int_A \int_\lambda H(\lambda)\, J(\lambda)\, d\lambda\, dA$$

$$= k\, AW \frac{\int_\lambda H(\lambda)\, j(\lambda)\, d\lambda}{\int_\lambda j(\lambda)\, d\lambda}$$

$$= k\, AW \left[\text{Relative Effectiveness of the Photocell}\right]$$

where A is the area of the cell.

Manufacturers normally specify curves relating i and W for a particular $j(\lambda)$ (usually the spectrum of the sun, or daylight) as well as the relative response $H(\lambda)$ of the photocell. These are shown below.

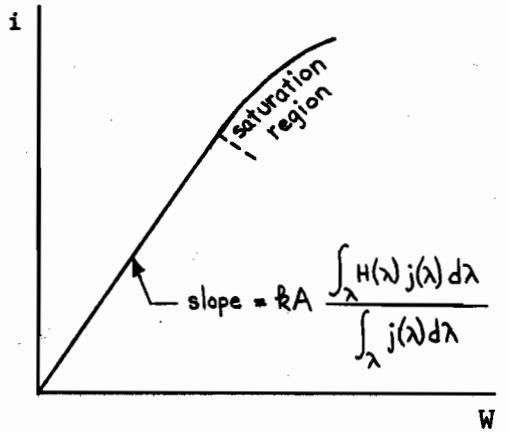

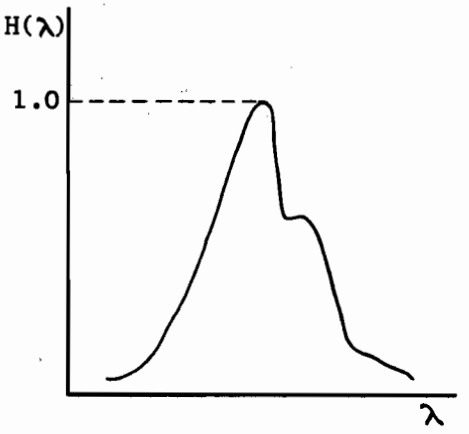

If a filter of response $G(\lambda,y,z)$ is included between the light and the cell then the current is

$$i = k W_p \frac{\int_A \int_\lambda G(\lambda,y,z)\, H(\lambda,y,z)\, j(\lambda,y,z)\, d\lambda\, dA}{\int_A \int_\lambda j(\lambda,y,z)\, d\lambda\, dA}$$

$$= k W_p \left[\text{Relative Effectiveness of the System}\right]$$

For light incident on the photocell at an angle these expressions must be modified unless all measurements are made at that angle.

BIBLIOGRAPHY

1. Van Slyke, D. D., and Neil, J. M.: Determination of Gases in Blood and Other Solutions by Vacuum Extraction and Manometric Measurements, J. Biol. Chem., 61:523, 1924

2. Drabkin, D. L., and Austin, J. H.: Spectrophotometric Studies I. Spectrophotometric Constants for Common Hemoglobin Derivatives in Human, Dog, and Rabbit Blood, J. Biol. Chem., 98:719, 1932

3. Drabkin, D. L., and Austin, J. H.: Spectrophotometric Studies V. A Technique for the Analysis of Undiluted Blood and Concentrated Hemoglobin Solutions, J. Biol. Chem., 112:51, 1935

4. Brinkman, R., and Wildschut, A. J. H.: A Clinical Method for Rapid and Accurate Determination of Oxygen Saturation in Small Amounts of Blood, Acta. Med. Scandinav., 94:459, 1938

5. Drabkin, D. L., and Singer, R. B.: Spectrophotometric Studies VI. A Study of the Absorption Spectra of Non-hemolyzed Erythrocytes and of Scattering of Light by Suspensions of Particles, with a Note upon the Spectrophotometric Determination of the pH Within the Erythrocyte, J. Biol. Chem., 129:739, 1939

6. Millikan, G. A.: The Oximeter, an Instrument for Measuring Continuously Oxygen Saturation of Arterial Blood in Man, Rev. Sci. Instr., 13:434, 1942

7. Goldie, E. A. G.: A Device for the Continuous Indication of Oxygen Saturation of Circulating Blood in Man, J. Sci. Instr., 19:23, 1942

8. Hemingway, A., and Taylor, C. B.: Laboratory Tests of the Oximeter with Automatic Compensation for Vasomotor Changes, J. Lab. and Clin. Med., 29:987, 1944

9. Drabkin, D. L., and Schmidt, C. F.: Spectrophotometric Studies XII. Observations of the Circulating Blood in Vivo, and the Direct Determination of the Saturation of Hemoglobin in Arterial Blood, J. Biol. Chem., 157:69, 1945

10. Roos, A., Elam, J. O., and Neville, J. F. Jr.: The Oximetric Determination of Cardiac Output in Man, Fed. Proc., 7:104, 1948

11. Wood, E. H., Geraci, J. E., and Groom, D. L.: Photoelectric Determination of Blood Oxygen Saturation in Man, Fed. Proc., 7:137, 1948

12. Hartman, F. W., et al.: A Photoelectric Oxyhemograph, a Continuous Method for Measuring the Oxygen Saturation of the Blood, Am. J. Clin. Path., 18:1, 1948

13. Knutson, J., Taylor, B. E., Wood, E. H.: The Oximetric Method for Determination of Oxygen Saturation of Mixed Venus Blood in Man, Fed. Proc., 8:87, 1949

14. Comroe, J. H., Wood, E. H.: Measurement of the Oxygen Saturation of Blood by Photoelectric Colorimeters (Filter Photometers), Methods in Med. Res. Vol. II, Yearbook Pub. 1949

15. Elam, J. O., et al.: Sources of Error in Oximetry, Ann. Surg., 130:755, 1949

16. Wood, E. H., Geraci, J. E.: Photoelectric Determination of Arterial Oxygen Saturation in Man, J. Lab. & Clin. Med., 34:387, 1949

17. Wood, E. H., Taylor, B. E., Knutson, J.: Oximetric Measurements of Circulation Time and Arterial Saturation Time During Oxygen Breathing in Man, Fed. Proc., 8:171, 1949

18. Wood, E. H.: The Oximeter, Medical Physics Yearbook Pub. 1949

19. Hartman, F. E., et al.: The Oxyhemograph, Am. J. Surg., 78:867, 1949

20. Brinkman, R., Zylstra, W. G.: Determination and Continuous Registration of the Percentage Oxygen Saturation in Small Amounts of Blood, Arch. chir. neerl., 1:177, 1949

21. Johnson, A. L., Stephen, C. R., Sekelj, P.: Clinical Use of the Oximeter, Can. Med. Assoc. J., 63:552, 1950

22. Wood, E. H.: A Single Scale Absolute Reading Ear Oximeter, Proc. Staff Meeting Mayo Clin., 25:384, 1950

23. Paul, W.: Contribution to Oximeter Design Using Modulated Light, Fed. Proc., 9:99, 1950

24. Stephen, C. R., Slater, Johnson, A. L., Sekelj, P.: The Oximeter - A Technical Aid for the Anesthesiologist, Anesthesiology 12:541, 1951

25. Sekelj, P., Johnson, A. L., Hoff, H. E., Schuerch, M. P.: Photoelectric Method for the Determination of Arterial Oxygen Saturation in Man, Am. Heart J., 42:826, 1951

26. Zylstra, W. G.: Fundamentals and Applications of Clinical Oximetry, Thesis Groningen, 1951

27. Paul, W., Grapes, B. G., Taplin, R. H.: Vascular Patterns in Ear as a Source of Error in Oximetry, Fed. Proc., 11:119, 1952

28. Perkins, J. F., Adams, W. E., Livingstone, H.: The Conversion of Millikan and Wood Type Oximeters into Direct-Writing Recording Instruments, J. Lab. & Clin. Med., 40:457, 1952

29. Rodrigo, F. A.: The Determination of the Oxygenation of Blood in Vitro by using Reflected Light, Am. Heart J., 45:809, 1953

30. Taplin, R. H., Saville, H. G., Paul, W.: Improved Earpieces for Oximeters, J. Aviation Med., 24:70, 1953

31. Paul, W.: An Oximeter For Continuous Absolute Estimation of Oxygen Saturation, J. Sci. Inst., 30:165, 1953

32. Sekelj, P.: Further Studies in Oximetry, Am. Heart J., 48:746, 1954

33. Paul, W.: Analog Computer for A-C Oximetry, J. Sci. Inst., 32:286, 1955

34. Sekelj, P., Johnson, A. L.: Photoelectric Method for Estimation of the Oxygen Saturation of Non-hemolyzed Whole Blood, J. Lab. & Clin. Med., 49:465, 1957

35. Kay, R. H., Coxon, R. V.: Optical and Instrumental Limitations to the Accuracy of "Oximetry", J. Sci. Instr., 34:233, 1957

36. Paul, W.: Oximetry, I.R.E. Trans. B.M.E., July 1958

37. Keilin, D., Hartree, E. F.: Spectrophotometric Study of Suspensions of Pigmented Particles, Biochimica et Biophysica Acta, 27:173, 1958

38. Sekelj, P., Jegier, W., Johnson, A. L.: Automatic Electronic Computer for the Estimation of Arterial Concentration of Evans Blue Dye, Am. Heart J., 55:485, 1958

39. Sekelj, P., Bates, D. V., Johnson, A. L., Jegier, W.: Estimation of Cardiac Output in Man by Dye Dilution Method Using an Automatic Computing Oximeter, Am. Heart J., 55:810, 1958

40. Nilsson, N. J.: Oximetry, Physiol. Rev., 40:1, 1960

41. Polanyi, M. L., Hehir, R. M.: New Reflection Oximeter, Rev. Sci. Instr., 31:401, 1960

42. Melville, A. W., et al.: An Improved Recording Oximeter, Electrical Engineering, May 1960

43. Sekelj, P., McGregor, M., Adam, W.: An Ear Oximeter for the Estimation of Coomassie Blue Dye in Blood, Proc. Third Int'l. Conf. on Med. El., London 1960

44. Anderson, N. M., Sekelj, P., McGregor, M.: The Transmission of Red and Infrared Light through the Human Ear, I.R.E. Trans. B.M.E.-8, No. 2, 1961

45. Sekelj, P., McGregor, M.: Estimation of Cardiac Output in Man Using an Ear Oximeter and Coomassie Blue Dye, I.R.E. Trans. B.M.E.-8, No. 2, 1961

46. Amesz, J., Duysens, L. N. M., Brandt, D. C.: Methods for Measuring and Correcting the Absorption Spectrum of Scattering Suspensions, J. Theoret. Biol., 1:59, 1961

47. Enson, Y., Briscoe, W. A., Polanyi, M. L., Cournand, A.: In Vivo Studies with an Intravascular and Intracardiac Reflection Oximeter, J. Appl. Physiol., 17(3):552, 1962